Identifying groundwater degradation sources in a Mediterranean coastal area experiencing significant multi-origin stresses

Lamine Boumaiza[1], Romain Chesnaux[1], Tarek Drias[2], Julien Walter[1], Frédéric Huneau[3,4], Emilie Garel[3,4], Kay Knoeller[5], Christine Stumpp[6]

[1] Université du Québec à Chicoutimi, Département des Sciences Appliquées, 555, boulevard de l'Université, Saguenay (Québec), G7H 2B1, Canada

[2] Université Mustapha Benboulaïd, Département de Géologie, Campus de Fesdiss, 05030 Batna, Algeria

[3] Université de Corse Pascal Paoli, Département d'Hydrogéologie, Campus Grimaldi, BP 52, F-20250 Corte, France

[4] CNRS, UMR 6134 SPE, BP 52, F-20250 Corte, France

[5] Helmholtz Centre for Environmental Research - UFZ, Department of Catchment Hydrology, Theodor Lieser Str. 4, Halle (Saale) 06120, Germany

[6] University of Natural Resources and Life Sciences, Institute for Soil Physics and Rural Water Management, Muthgasse 18, 1190, Vienna, Austria

Abstract

This study investigates the multiple contamination sources of a coastal Mediterranean aquifer in northeastern Algeria that is bordered by two rivers and neighboring densely populated areas. Hydrogeochemical and isotopic groundwater characterization is carried out, including the analyses of major elements, water stable isotopes $\delta^{2}H$-H_2O and $\delta^{18}O$-H_2O, and stable isotopes of nitrate $\delta^{15}N$-NO_3 and $\delta_{18}O$-NO_3, and then integrated into the history of land use over the study area. Groundwater nitrate concentrations ranging from 1.6 to 235 mg/L with a median value of 69 mg/L are evidence of the degradation of groundwater quality induced by anthropogenic sources. The combined of $\delta^{15}N$-NO_3 and $\delta_{18}O$-NO_3 ratios showed that nitrate in groundwater is attributable to (i) the uncontrolled development of inadequate private sanitation systems over the study area, and (ii) the unsafe application of animal manure to fertilize crops. Very active saltwater intrusion is confirmed by several hydrogeochemical indicators. Interestingly, the intrusion mechanism appears to be more complex than a direct intrusion from the Mediterranean Sea. During the high-water period, saltwater intrusion may also originate from the two rivers bordering the aquifer, via upstream migration of seawater through the river mouths. The heavier ratios in $\delta^{2}H$-H_2O and $\delta^{18}O$-H_2O of surface water collected from the rivers suggest that water from the Mediterranean Sea is mixing with water in the rivers. Multi-source contamination not only contributes to complex chemical reactions within the aquifer, but also contributes, via the cumulative effect of the various sources, to affecting large parts of the study area. The present study may serve as a warning to the effect that historical land-use practices may exert seriously deleterious impacts on groundwater quality and greatly limit conditions for the sustainable management of Mediterranean coastal areas.

Keywords
Aquifer, stable isotopes, nitrate, seawater intrusion, groundwater contamination, hydrogeochemistry, North Africa

1 Introduction

Worldwide, coastal areas have become increasingly urbanized. Accounting for approximately 10% of the Earth's surface, they are host to more than half of the world's population and human activities (Chatton et al., 2016). The socio-economic development in these coastal areas relies heavily on the availability of water resources, including groundwater. Groundwater resources are subjected to very strong stressors due to their often uncontrolled overuse for domestic, agricultural, industrial, and mass tourism purposes. Poor groundwater management combined with other deleterious practices in areas such as domestic sewage systems results in groundwater quality degradation, which often leads to (i) heavy contamination of groundwater particularly by nitrate (Chafouq et al., 2018; Cheema et al., 2014; Leaney et al., 2004; Sdao et al., 2012; Senthilkumar et al., 2018; Shi et al., 2018; Shuler et al., 2017), and (ii) salinization due to seawater intrusion into aquifers, enhanced by excessive pumping of groundwater (Chaouni et al., 1997; Custodio, 2002; Faye et al., 2005; Khayat et al., 2006; Steyl and Dennis, 2010). Seawater intrusion remains a severe threat to coastal aquifers (Michael et al., 2017), particularly in a context where climate change exerts multiple combined effects, including sea level rise and coastal erosion (Ketabchi et al., 2016; Klassen and Allen, 2017; Lemieux et al., 2015). Developing effective management practices whose aim is to preserve groundwater quality requires identifying groundwater contamination sources and understanding the processes that control the evolution of groundwater quality (including the geochemical and hydraulic connectivity between groundwater and groundwater-dependent ecosystems). Groundwater quality in aquifers is mainly controlled by two factors: (1) natural processes related to the aquifer including lithology, recharge quality, groundwater

flow, residence time and soil/rock interactions with water (Ledesma-Ruiz et al., 2015; Walter et al., 2017); and (2) anthropogenic activities including agricultural practices, industrial wastewater discharges, domestic sewage practices, dumping sites, animal wastes, etc. (Böhlke, 2002; Erostate et al., 2018; Garewal and Vasudeo, 2018; Hudak, 2000; Lu et al., 2008; Nolan, 2001; Singh et al., 1995; Stigter et al., 1998). Due to the shallow depth of groundwater in coastal aquifers, surface anthropogenic contamination sources play a major role in groundwater contamination in these aquifers (Ntanganedzeni et al., 2018). It is a challenging task to identify groundwater contamination sources and understand the processes that control the evolution of groundwater quality in coastal areas where land use is diverse and is subject to multiple potential inputs.

Many studies focussing on the degradation of groundwater quality, including those observed in coastal aquifers, pay particular attention to nitrate contamination (Beeson and Cook, 2004; Burden, 1982; Fukada et al., 2004; Jin et al., 2012; Minet et al., 2017; Pastén-Zapata et al., 2014; Rao, 2006). Excessive consumption of nitrate in drinking water has been associated with the risk of ‘‘methemoglobinemia’’ known as ‘‘blue baby syndrome’’, as well as stomach cancer (Fan and Steinberg, 1996; Greer and Shannon, 2005). From an environmental perspective, the discharge of nitrate into surface water bodies could lead to planktonic and algal blooms, which result in eutrophic conditions, often followed by major reductions of fish stocks and other aquatic life due to oxygen depletion (Kendall, 1998; Mason, 2002; Vitousek et al., 1997). Partial denitrification of nitrate in groundwater introduces nitrous oxide, which is a powerful greenhouse gas (Sutton et al., 2011). Consequently, to evaluate and predict environmental and health risks, it is necessary to identify the sources of nitrate, as well as its transport

process and fate (Kopáček et al., 2013). Historically, agricultural practices have been considered as the principal source of nitrate, since intense use of synthetic and animal waste fertilizers in agricultural areas have been shown to contribute up to 80% of the reactive nitrogen produced worldwide (Erisman et al., 2008). However, direct application of nitrogen-based fertilizers to agricultural lands is not the only source. Wastewater discharges from treatment plants, septic tanks (Wakida and Lerner, 2005) and leaking sewers (Gooddy et al., 2014), as well as sludge and seepage from landfills (Christensen et al., 2001) could also contribute nitrate to groundwater. Many studies focussing on the identification of nitrate sources have shown that nitrate is not only associated with the use of fertilizers (Jin et al., 2012; Matiatos, 2016; Pastén-Zapata et al., 2014; Stoewer et al., 2015; Vystavna et al., 2017). Wang et al. (2017) examined sources of nitrate in areas with diverse land uses; these authors highlighted the importance of controlling nitrate sources through the careful application of manure-based fertilizers and control of septic leakage. High concentrations of nitrate in groundwater are typically observed in intensive agricultural areas with high human population densities. In most cases, land use is the dominant factor controlling nitrate concentrations in groundwater, because nitrate migrates by vertical transport through the vadose zone and is then transported via groundwater flow. Consequently, establishing a reliable conceptual hydrogeological model that represents groundwater flow paths combined with nitrate sources that have been identified as well as their spatial distribution is necessary to better understand the dynamics of nitrate contamination. But in areas with multiple land uses, determining nitrate sources is often challenging due to a broad variety of potential sources. Stable isotope ratios of nitrogen ($\delta^{15}N\text{-}NO_3$) and oxygen ($\delta^{18}O\text{-}NO_3$) of nitrate can be used to

investigate nitrate sources (Böttcher et al., 1990; Kendall, 1998; Pastén-Zapata et al., 2014; Stoewer et al., 2015; Wassenaar, 1995). The interest in using these stable isotopes resides in the expectation that some of the major nitrogen sources involved in the terrestrial nitrogen cycle are able to provide valuable recognizable distinct isotope signatures in groundwater (Kendall et al., 2007; Seiler, 2005). The combined analysis of $\delta^{15}N\text{-}NO_3$ and $\delta^{18}O\text{-}NO_3$ makes it possible to distinguish various potential sources such as fertilizers, soil organic matter, and animal manure/septic sewage effluents (Baily et al., 2011; Kendall, 1998; Panno et al., 2001). Furthermore, the combined use of $\delta^{15}N\text{-}NO_3$ and $\delta^{18}O\text{-}NO_3$ constitutes a viable tool to trace nitrate transformation processes such as denitrification (Böttcher et al., 1990; Wassenaar, 1995).

The intensive extraction of groundwater from coastal aquifers reduces freshwater outflow to the sea and depresses the local water table, causing seawater to migrate further inland toward aquifers (Bear et al., 1999). This phenomenon has been observed in many coastal areas worldwide (Bocanegra et al., 2010; Mas Pla et al., 2014; Seddique et al., 2019; Werner, 2010) and is an important environmental issue negatively affecting groundwater resources. Salinity degrades the quality of groundwater and therefore reduces the volume of freshwater that is available (Post, 2005; Ros and Zuurbier, 2017; Werner et al., 2013). The addition to freshwater of seawater in a proportion equivalent to less than 1% (≈ 250 mg/L chloride) renders freshwater unfit for drinking (WHO, 2017). In the Western Mediterranean countries, including Algeria, Alfarrah and Walraevens (2018) reported several cases of seawater intrusion into coastal aquifers. This alarming situation introduced negative effects including a transformation of land use in traditionally agricultural areas, as a consequence of saltwater contamination of

agricultural land potential. Studies of seawater intrusion into coastal aquifers is essential in identifying affected areas and potentially preventing problems (Alfarrah and Walraevens, 2018). The degree of seawater intrusion depends on the balance between an aquifer's recharge capability and the quantities of groundwater that are extracted, as well as the hydrogeological parameters controlling groundwater flow within the aquifer. In addition, climate change and particularly sea-level rise exert a negative impact. It is essential to understand the complex interactions between groundwater, surface water and seawater in order to be able to effectively manage the groundwater resource in a coastal aquifer.

Many methods can be used to investigate the extent of seawater intrusion, including head measurements (e.g. Post, 2005), geophysical methods (e.g. Choudhury et al., 2001), geochemical methods (e.g. Giménez-Forcada and Sánchez San Román, 2015), analytical solutions (e.g. Pool and Carrera, 2011) and numerical modeling using for example the SEAWAT software (Langevin et al., 2007). Because groundwater can record past anthropogenic contaminations that have influenced an aquifer's drainage area over long time periods, they have been shown to behave as a sort of "environmental archive". Geochemical techniques have been widely used to identify the origin of salinity and to trace the evidence of seawater intrusion through coastal aquifers (Eissa et al., 2014; Giménez-Forcada, 2019; Han and Currell, 2018; Kim et al., 2003; Nair et al., 2015). These techniques are particularly valuable as the dynamic of seawater intrusion in coastal aquifers can be complex and may involve multiple salinization processes occurring simultaneously (Han and Currell, 2018).

The main goal of the present study is to present a case study of a shallow coastal aquifer neighboring an expanding urban area in which are identified the major hydrogeochemical processes controlling the degradation of groundwater quality. The adopted methodology was to combine the study of geochemical factors (major elements) with the study of environmental isotopes ($\delta^{2}H$-H_2O, $\delta^{18}O$-H_2O, $\delta^{15}N$-NO_3, and $\delta_{18}O$-NO_3) and historical data on land use. The specific objectives were to identify nitrate sources as well as the processes controlling its evolution within the aquifer, and to understand the process of groundwater salinization within the aquifer. Ultimately, it is hoped that the adopted methodology may improve our ability to predict the impact of global change on coastal aquifers.

2 Description of the study area

2.1 *Geographic location and climate*

The expanding urban coastal area of Taleza is located in northeastern Algeria. It is one of the districts of the municipality of Collo in the Skikda region (Figure 1). It is crossed by a national road (N-85) connecting Collo with the municipality of Kerkera. The study area is surrounded by hills whose altitude varies from 200 to 600 m, except the southeast boundary where the study area is connected with a large flat valley. Further North, the expanding urban area of Taleza is bordered by the Mediterranean Sea over a shoreline of roughly 3 km. The study area takes the general form of a flat alluvial system covering a surface of approximately 8 km^2, with a slight downhill sloping going northward toward the Mediterranean Sea.

The climate of the study area is typically Mediterranean. The average determined monthly temperature is 10.6 °C in winter and 27.5 °C in summer, with a mean annual

relative humidity of about 68 % (Beloulou, 1987). The expanding urban area of Taleza is fed by precipitation (800 to 1000 mm/year), runoff from surrounding metamorphic hills (2000 mm/year), and infiltration influx from the Guebli River which drains a large sub-watershed covering an area of 993 km^2 (Mecibah, 2008). The Cherka River, which drains a local watershed located in the western part of the study area, also constitutes a feeding source of water infiltration into geological formations under the study area.

2.2 *Geology*

The study area is a delta valley that belongs to the Petite Kabylie region in north-eastern Algeria, bordering the Mediterranean Sea and extending southwards to the coastal magmatic range of the Babor Mountains. This region has been the subject of several geological investigations, including by Bouillin and Kornprobst (1974), Bouillin (1979), and Marre (1987). Minmeliovodkhoz (1968) mapped the surface geological deposits of the study area and of its surrounding regions (Figure 2). Several Quaternary deposits (silt sandy clay, clayey silt and sand) cover the mapped surface area; the specific study area is mostly dominated by a silt sandy surface deposit with a sandy shoreline band (Figure 2). The deeper geological material under the expanding urban area of Taleza was identified by studies on cross-sections conducted by 1) the General Company of Geophysics whose investigators successfully applied the resistivity method (CGG, 1965), 2) a Soviet mission as part of an irrigation project (Minmeliovodkhoz, 1968), and 3) the Algerian National Agency for Hydraulic Resources as part of a hydrogeological study (ANRH, 1974). The deeper material is constituted of a heterogeneous Quaternary granular alluvium deposit that varies in thickness between 5 and 40 m, resting on marl Mio-Pliocene substratum (Figure 2).

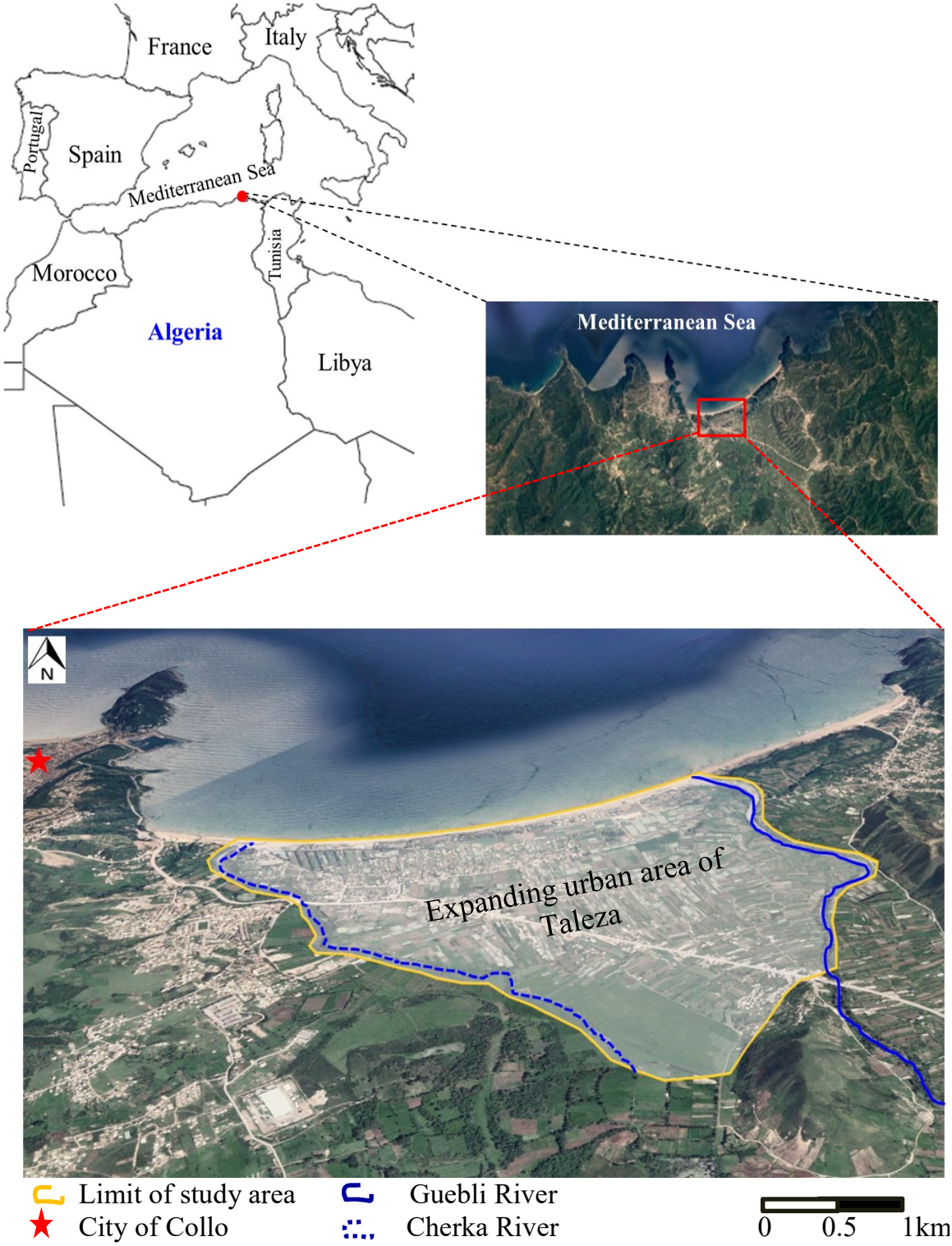

Figure 1. Geographic location of study area with a perspective overview.

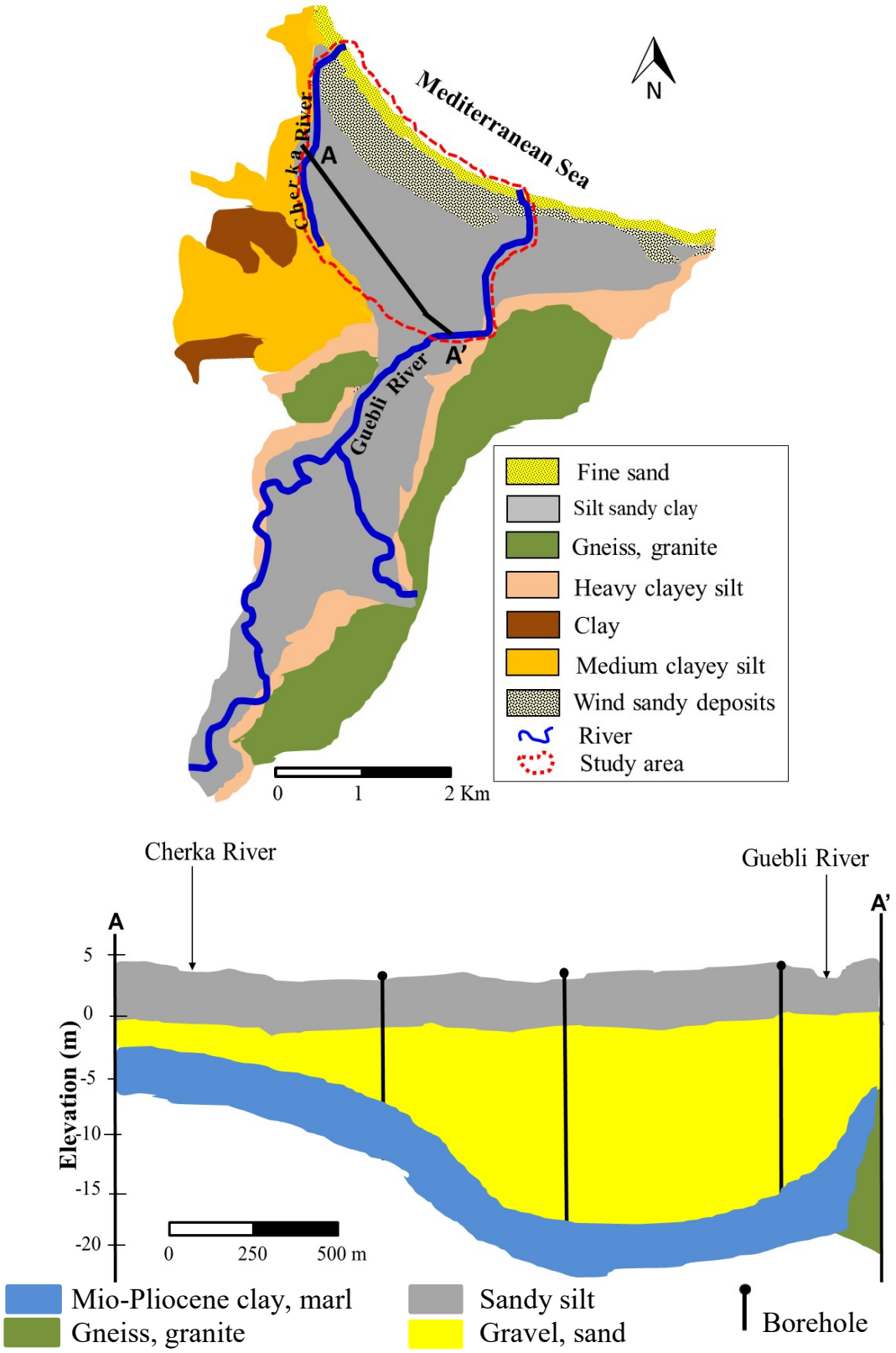

Figure 2. Surface geological deposits of the Taleza region (Minmeliovodkhoz, 1968), and cross-section AA' conducted in the study area by ANRH (1974).

2.3 *Hydrogeological background*

The expanding urban area of Taleza overlies an unconfined granular aquifer measuring approximately 8 km^2 that constitutes an important groundwater reservoir. The alluvial deposits correspond to a highly permeable unconfined aquifer. The hydraulic conductivity of this aquifer was estimated to vary between $8.29x10^{-4}$ m/s and $2.07x10^{-3}$ m/s based on pumping test data according to Jacob's method (Jacob, 1947) for two municipal wells located in the southeastern section of the expanding urban area of Taleza (Beloulou, 1987). Before the development of significant human activity in the Taleza region in the 1960's and 1970's, the effective volume of the groundwater reservoir of the Taleza aquifer was estimated to be approximately 75 million cubic meters (CGG, 1965). De-Camps (1974) had estimated at 120 L/s the potential extraction flow rate from this aquifer. Given that historically, the aquifer was subjected to a low pumping rate (48 L/s), the issue of seawater intrusion had been ignored by most of the studies conducted in the 1960's and 1970's (Krom 1965; Grenet 1972; De-Camps 1974), with the exception of the study conducted by CGG (1965), which indicated that the sector bordering the Mediterranean Sea, for about 600 m, revealed values of transversal electrical resistance (the product of the resistivity and the saturated thickness of the material) that were much lower than those measured elsewhere in the aquifer. This observation indicates that freshwater is probably affected by saltwater because if the aquifer were saturated only with freshwater, the transversal electrical resistance values would have been much higher (Beloulou, 1987). The coastal aquifer of Taleza was also considered by Boulabeiz et al. (2018) to be highly vulnerable to seawater intrusion, based on a GIS-based GALDIT model.

2.4 *Land use time-evolution and anthropogenic contamination*

Historically, the first settlements in the area of Taleza were located in its northwestern portion (named previously Ouled-Mazouz), and to a lesser extent, in its southeastern area named El-Tahra Hill-territory (Figure 3). Given its low population density, the plain of Taleza was then dominated by large agricultural zones of arable lands occupying more than 90% of the total surface. But since the late 1990s, the plain of Taleza has been increasingly and intensively urbanised; many private homes were randomly constructed in the Ouled-Mazouz sector, from the northwestern to the northeastern areas of the plain (Figure 4). Other areas where housing developments have been established in an uncontrolled manner include the borders of the national road (N-85) that crosses the plain of Taleza (Figure 4). More recently, many large residential housing areas were built by the Algerian Government in different locations of the expanding urban area of Taleza. These have been connected to local sewage collection and storage systems. In addition, the northern sector of the plain hosts a tourism development zone bordering the Mediterranean Sea (Figure 3), where resorts, hotels and other facilities have been constructed (Chabour et al., 2009). The urban area of Taleza is more active in the summer period, ranging from May to August, when people from the surrounding provinces (e.g., Constantine, Batna, Biskra, Oum El-Bouaghi, Khenchela) come to spend their vacation on the shores of the Mediterranean Sea. Ferah (2015) mentioned that an average of 600,000 tourists per year visit the beach of the urban area of Taleza. This number of temporary visitors in the area is added to permanent residents, whose population is also strongly increasing. The number of permanent inhabitants has been multiplied by 7 between 1962 and 2014 (Ferah, 2015).

Despite being the site of a marked urbanisation trend, the total surface of the study area is still made up approximately of 60% of agricultural lands (Figure 3). Except for the southwestern area which is dominated by cereal production (representing approximately 10% of the arable lands), the agricultural activities are mostly dominated by production of legumes under commercial plastic greenhouses and in open agricultural fields. The dual impact of agriculture and the randomly developing urban sprawl in Taleza have motivated a number of investigations on consecutive contamination, wherein nitrate concentrations in groundwater have been used as an indicator (e.g., Boulabeiz, 2006; Hamani, 1998) of degrading groundwater quality. The high concentrations of nitrate observed in groundwater under the plain of Taleza have coincided with specific locations of agricultural areas and sectors with intense population densities. Unsafe agricultural practices and inadequate private sanitation systems combined with the absence of a proper sanitation network have been presumed to be the principal sources of nitrate in groundwater (Boulabeiz 2006). Despite these encroachments on its quality, the coastal aquifer of Taleza still constitutes a significant source of water supply. Eight municipal wells were installed in the plain of Taleza between 1965 and 1987, and these were used to supply water to surrounding communities (Collo, Ain-Aghbel and Kerkra) before potable water gradually became available in 1993 from the treated surface water of the Beni-Zid Dam (Chabour, 2004). Since then, the growth of urbanization over the expanding urban areas of Taleza has generated uncontrolled drilling by the population of an excessive number of private wells for many different purposes, including drinking water. As a consequence of all these developments over the last 30 years, the salinity of groundwater within the coastal aquifer of Taleza was presumed to be the result of

excessive exploitation of groundwater over a long period of time (Chabour et al., 2009). More recently, some residents have noted the presence of an unpleasant odor resembling that of rotten eggs in the groundwater pumped from their wells (Boumaiza et al., 2019a). Another type of groundwater contamination may be occurring as a result of the possible influx into the aquifer of surface waters from the two rivers that border the valley, namely the Cherka and Guebli rivers (Boulabeiz, 2006). The Guebli river is 154 km long and has been the site of various industrial and commercial spills. This river is also used as an outlet for the sewage systems of many cities upstream. Waste waters are being poured into this river without any prior treatment. The Cherka river is a large receptor for various wastes, such as used oils, garbage, concrete and rubble. Also, the sanitation network of the City of Ramoul-Abdelazize (with a population of more than 8,000 persons), drains into this river without any prior treatment (Boumaiza et al., 2019b).

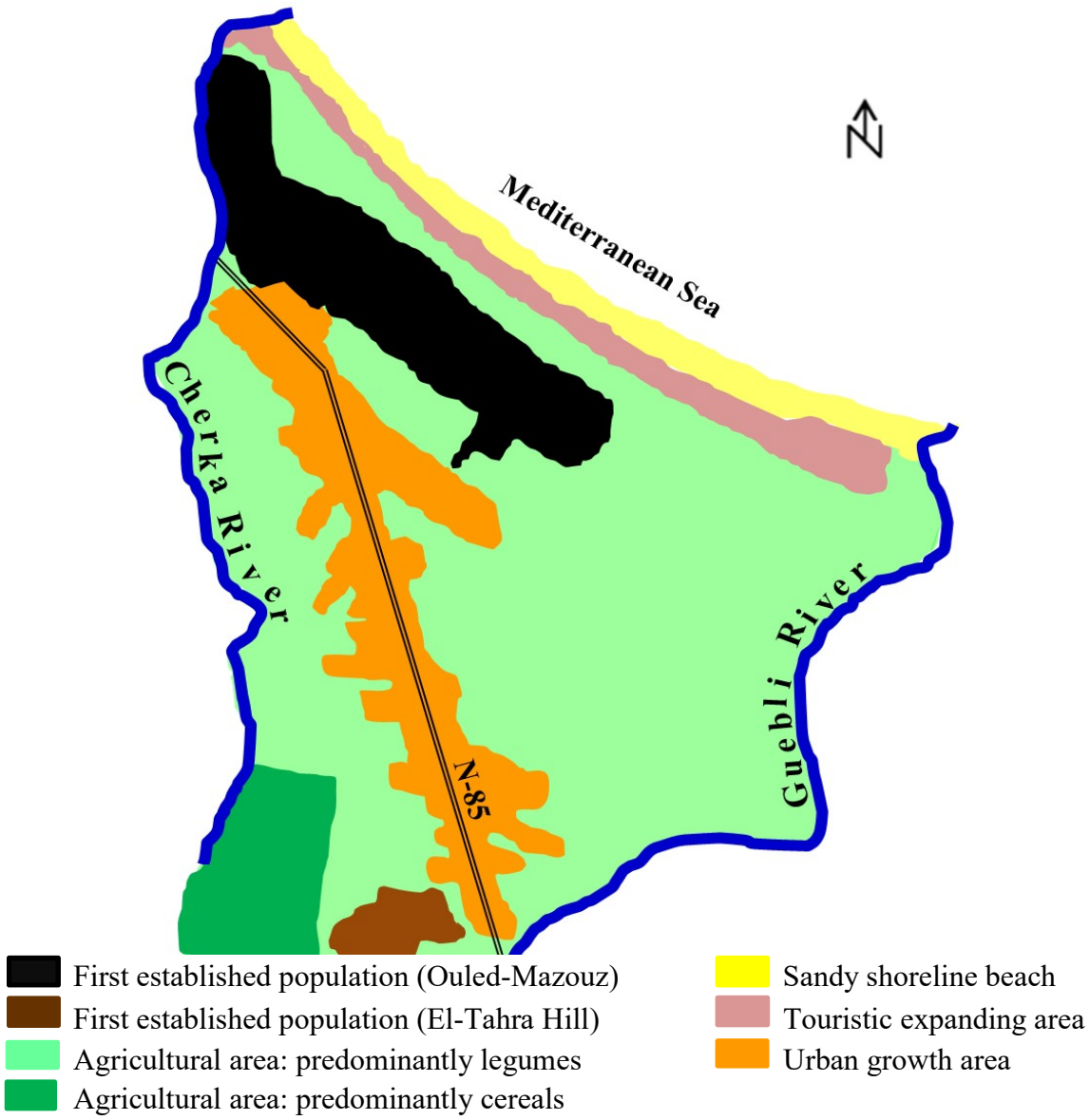

Figure 3. Land-use map and population density in the expanding urban area of Taleza

(a) (b)

Ouled-Mazouz sector

Housing development bordering the national road (N-85)

Figure 4. Uncontrolled housing developments in the study area: (a) situation in 2003, and (b) situation in 2020.

3 Material and methodology

3.1 Sampling and laboratory analyses

3.1.1 Sampling network

For this study, a comprehensive sampling campaign, including piezometric measurements, was conducted on June 11 to 16, 2019. The single exception is a sample collected on November 15th, 2019 from the Mediterranean Sea (TAL-32) to obtain stable isotopes of nitrate. The sampling program included twenty-seven groundwater samples distributed more or less evenly over the entire study area, four surface water samples collected from the Guebli and Cherka Rivers (two samples at each river), as well as the

aforementioned water sample collected from the Mediterranean Sea far from the outlet of the rivers (Figure 5). The groundwater samples were collected from existing private wells (these were shallow at an average depth of 2.4 m below ground surface, with a diameter varying overall from 2 to 3 m). Prior to sampling, stagnant groundwater present in the bottom of the private wells was purged using a pumping system. The physico-chemical parameters (temperature (T), pH and electrical conductivity (EC)) of the fresh groundwater were monitored, using a Hanna HI-9812-5 Portable Meter, until three consecutive readings stabilized within ±10%. Groundwater sampling was then performed at the discharging pipe of the pumping system. For the five surface water samples (one from the sea and two from each river), the water was collected some meters (2 to 3 m) below the surface using a Waterra foot pump valve system attached to a pipe.

The samples destined for major anion and cation analysis were filtered in-situ through 0.45-µm nitrocellulose membrane filters with 100 mL luer-lock syringes, before collection in two 40-mL amber glass bottles. One of these two bottles (for cation analysis) was acidified to pH <2 by adding 2 to 3 drops of ultrapure nitric acid (HNO_3). The water destined for δ^2H-H_2O and $\delta^{18}O$-H_2O analyses was collected in two 40-mL amber glass bottles, while the water destined for $\delta^{15}N$-NO_3 and $\delta^{18}O$-NO_3 measurement was collected in two 50-mL polyethylene bottles. All samples were collected in bottles without head-space; furthermore, these bottles were equipped with caps containing Teflon septa parafilm to avoid evaporation. During fieldwork, the samples were stored in a cooler at 4°C, before being stored in a refrigerator (4°C), and further transported to the laboratory. The water samples collected for the measurement of stable isotopes of nitrate were stored in a frozen state until the analyses were completed.

Figure 5. General location of groundwater samples and surface water samples collected from the Guebli River (identified as #26 and #27), from the Cherka River (identified as #28 and #29), and from the Mediterranean Sea (identified as #32).

3.1.2 Hydrogeochemical and stable isotope analyses

The $\delta^{2}H$-H_2O and $\delta^{18}O$-H_2O ratios, as well as the major chemical elements (bicarbonate (HCO_3^-), bromide (Br^-), nitrate (NO_3^-), chloride (Cl^-), potassium (K^+), magnesium (Mg^{2+}), ammonium (NH_4^+), sodium (Na^+), calcium (Ca^{2+}) and sulfate (SO_4^{2-})) were analyzed at the Hydrogeology Department of the University of Corsica (France). HCO_3^-

was determined by volumetric titration, with a digital titrator HACH (Hach Company, Loveland, CO, U.S.A), while the concentrations of the other major chemical elements were determined using a Dionex ICS 1100 chromatograph (Thermo Fischer Scientific, Waltham, USA). The $\delta^{2}H\text{-}H_2O$ and $\delta^{18}O\text{-}H_2O$ ratios were determined using a laser-based liquid-vapour stable isotope analyser DLT-100 (Los Gatos Research, San Jose, USA). Stable isotopes of nitrate $\delta^{15}N\text{-}NO_3$ and $\delta^{18}O\text{-}NO_3$ were analyzed at the Helmholtz Center for Environmental Research in Halle/Saale (Germany), using the denitrifier method (Casciotti et al., 2002; Sigman et al., 2001). This method was performed using the *Pseudomonas chloroaphis subsp. auerofaciens* (ACT 13985 equal to DSM-6698) strain according to the protocols of Casciotti et al., (2002) and Sigman et al., (2001). All groundwater samples were analyzed for stable isotopes of nitrate, except the groundwater sample TAL-1 due to a technical issue. It should also be noted that in the end, only one surface water sample was analyzed from each river. Stable isotope ratios are expressed in δ‰ relative to the international reference of Vienna Standard Mean Ocean Water (VSMOW). The isotope ratios were calculated using the following equation (Eq. 1):

$$\delta = \frac{R_{sample} - R_{standard}}{R_{standard}} \quad (1)$$

where R_{sample} represents either the $^{18}O/^{16}O$ or the $^{2}H/^{1}H$ ratio of the water sample, while $R_{standard}$ is the $^{18}O/^{16}O$ or the $^{2}H/^{1}H$ ratio of the VSMOW. The distribution of isotopic ratios of the collected water samples is compared to the range of Local Mediterranean Meteoric Water Line (LMMWL) values derived from d-excess values, ranging from 14‰ to 27‰, proposed by Gat et al. (2003) for the Mediterranean area closest to the study area.

3.2 **Methods used to evaluate seawater intrusion**

3.2.1 Hydrochemical facies evolution diagram

The hydrochemical facies evolution diagram (HFE-D) provides a straightforward method to identify the phases of a coastal aquifer (facies) that are subject to saltwater intrusion or freshening or intermediate phases between the two. These can be identified by analyzing the distribution of anion and cation percentages in the diagram. The intrusion process can be summarized as seawater migrating from the ocean towards the aquifer; once inside the aquifer, the saltwater mixes with the freshwater already in place through recharge. Seawater intrusion includes several secondary processes that develop as a consequence of the change in groundwater chemistry (Giménez-Forcada, 2019). By entering the anion and cation concentrations of the water samples into the HFE-D, a conservative mixing line (CML) can be established to separate the freshening phase from the seawater intrusion phase. The facies types situated above and to the left of the CML are representative of the freshening phase, including its sub-stages (f1, f2, f3, f4 and freshwater (FW)), while facies types located below and to the right of the CML represent the seawater intrusion phase, including its sub-stages (i1, i2, i3, i4 and saltwater (SW)). Facies located in the center can belong to either the freshening or seawater intrusion phases, but this depends on their position compared to the CML, and therefore, on the chemical composition of freshwater (Giménez-Forcada and Sánchez San Román, 2015).

3.2.2 WSDE graphic approach

A graphic approach to seawater intrusion analysis was proposed as an alternative by the Washington State Department of Ecology (WSDE, 2005). This approach consists in

plotting Cl^- concentrations (mg/L) versus EC (μS/cm) to determine the condition of water according to three zones (normal water, mixed water, and seawater intrusion) shown in the graph. Groundwater samples characterized by Cl^- concentrations of 100-200 mg/L and EC of 600-2000 μS/cm represent a mix of freshwater and saltwater, whereas groundwater characterized by Cl^- concentrations exceeding 200 mg/L and EC exceeding 1,000 μS/cm are most likely influenced by seawater intrusion.

3.2.3 Seawater mixing index

Seawater mixing index (SMI) is an effective tool for estimating the relative degree of seawater mixing (Park et al., 2005). This index is based on the concentrations of four major ionic constituents of seawater (Na^+, Cl^-, Mg^{2+}, and SO_4^{2-}). The SMI can be calculated using Eq. 2.

$$SMI = a.\frac{C_{Na}}{T_{Na}} + b.\frac{C_{Mg}}{T_{Mg}} + c.\frac{C_{Cl}}{T_{Cl}} + d.\frac{C_{SO4}}{T_{SO4}} \quad (2)$$

where *a*, *b*, *c* and *d* are constants of 0.31, 0.04, 0.57 and 0.08, respectively, denoting the relative concentration proportion of Na^+, Cl^-, Mg^{2+}, and SO_4^{2-} in seawater. *C* is the measured concentration of these ions in mg/L. *T* represents the regional threshold values of the considered ions, which can be determined as the inflection points from the cumulative probability curves for the concentrations of Na^+, Cl^-, Mg^{2+}, and SO_4^{2-} in groundwater samples (Sinclair, 1974). An SMI value >1 denotes groundwater that is influenced by seawater mixing with freshwater. Otherwise, a value lowers than 1 for SMI denotes freshwater.

4 Results and discussion

4.1 Evidence of multiple sources of mineralization

A summary of the hydrogeochemical and stable isotope concentrations of groundwater and surface water is presented in Table 1. A bivariate correlation approach is first used to determine the principal source of salinity based on EC, assuming that a correlation factor R^2>0.5 indicates a significant level of correlation (Barthold et al., 2011; Gilabert-Alarcón et al., 2018). Second, a correlation factor is used for a preliminary evaluation of the hydrochemical origin of the facies and to suggest possible geochemical processes which may explain the origin of the water (Section 4.2.1). EC shows a good correlation with Cl^-, Br^-, Na^+, and Mg^{2+} (Table 2) suggesting that these elements are the principal sources of mineralization (Bouzourra et al., 2015). The presence of multiple sources of mineralization is also verified using the coefficient of variation (CV), which represents a standardized measure of dispersion of a probability distribution or a frequency distribution. This coefficient is widely used in analytical geochemistry to express the precision and repeatability of an essay. For one chemical element, CV is defined as the ratio of its standard deviation (SD) to the average value of concentrations recorded for this chemical element. Generally, a CV closer to zero indicates that the population is not dispersed and is homogeneous. Table 3 indicates that in the Taleza samples, the concentrations for chemical elements, with a high correlation factor with EC, are heterogeneous according to high values of CV; Karroum et al. (2017) have proposed that this type of result suggests that mineralization has multiple sources.

Table 1. Summary of the hydrogeochemical and stable isotope concentrations of groundwater and surface water samples

ID	T (°C)	pH	EC (µS/cm)	TDS [1] (mg/L)	HCO_3^- (mg/L)	Cl^- (mg/L)	Br^- (mg/L)	NO_3^- (mg/L)	SO_4^{2-} (mg/L)	Na^+ (mg/L)	$NH4^+$ (mg/L)	K^+ (mg/L)	Mg^{2+} (mg/L)	Ca^{2+} (mg/L)	δ^2H-H_2O (‰)	$\delta^{18}O$-H_2O (‰)	d-excess (‰)	$\delta^{15}N$-NO_3 (‰)	$\delta^{18}O$-NO_3 (‰)
TAL.1	20	7.4	1870	1403	671	361.3	1.8	9.1	51.9	237.6	3.2	7.7	49.3	112.4	-33.7	-6.35	17.0	-	-
TAL.2	20	7.3	590	443	207	63.6	0.3	63.4	41.9	41.8	0.7	5.9	13.3	68.6	-32.8	-5.85	13.9	9.7	5.3
TAL.3	18	7.4	840	630	415	67.1	0.4	33.3	54.9	49.0	b.d.l	1.5	18.2	114.0	-33.5	-6.07	15.1	3.7	5.5
TAL.4	21	7.1	1480	1110	500	199.7	1.3	5.8	45.5	95.9	1.6	4.2	38.4	178.9	-35.5	-6.60	17.3	15.4	12.3
TAL.5	20	7.3	850	638	415	76.3	0.5	34.2	47.8	50.0	b.d.l	3.3	19.9	119.7	-33.5	-6.34	17.2	9.7	5.5
TAL.6	21	7.3	810	608	207	167.5	0.7	70.2	101.6	41.5	b.d.l	1.6	19.2	129.9	-33.9	-6.41	17.3	8.4	5.0
TAL.7	20	7	690	518	366	50.2	0.4	26.6	28.8	45.2	0.4	1.3	18.7	95.4	-33.3	-5.83	13.3	14.1	4.9
TAL.8	20	7.2	710	533	183	53.4	0.3	103.7	69.7	39.5	0.2	2.9	15.7	88.0	-32.8	-5.92	14.5	2.0	2.3
TAL.9	20	7	510	383	171	59.4	0.3	48.7	27.9	34.7	0.4	2.6	11.9	55.2	-33.9	-6.50	18.1	10.2	5.5
TAL.10	19	7.3	1140	855	378	155.1	0.8	96.1	53.2	82.6	b.d.l	3.6	19.7	132.0	-32.6	-5.90	14.6	10.3	8.7
TAL.11	20	7.4	1060	795	366	63.4	0.4	49.2	65.6	75.7	b.d.l	6.6	15.0	122.6	-32.6	-6.26	17.5	10.5	4.4
TAL.12	19	7.2	1050	788	366	107.9	0.6	11.9	104.6	70.3	b.d.l	2.6	27.0	129.8	-34.0	-6.53	18.2	19.9	12.7
TAL.13	19	7.1	1660	1245	195	257.9	1.5	1.6	98.8	131.1	b.d.l	2.4	16.8	78.6	-33.3	-6.34	17.4	19.0	11.3
TAL.14	20	7.4	1000	750	366	117.3	0.7	99.4	43.5	83.4	b.d.l	14.8	16.9	99.3	-31.5	-5.78	14.7	11.2	5.3
TAL.15	21	7.2	1220	915	268	120.6	0.6	235.0	118.4	87.4	b.d.l	12.6	24.8	149.9	-31.7	-5.89	15.4	12.1	7.4
TAL.16	22	7.5	1180	885	610	63.4	0.4	49.4	65.2	107.1	0.3	11.1	23.9	169.6	-32.5	-6.07	16.0	16.9	6.6
TAL.17	19	7.3	1050	788	378	89.2	0.5	97.3	95.0	85.9	2.3	10.4	17.1	117.9	-30.9	-5.85	15.8	11.1	2.0
TAL.18	22	7.1	1300	975	500	175.4	0.9	22.1	92.9	104.4	1.2	4.3	37.8	144.2	-34.2	-6.65	19.0	15.5	6.4
TAL.19	20	7.3	850	638	366	57.4	0.4	98.3	63.8	38.6	b.d.l	7.9	16.9	119.7	-35.6	-7.04	20.7	11.7	5.8
TAL.20	21	7.2	540	405	122	53.6	0.3	68.5	60.9	34.9	0.3	2.4	11.3	61.6	-34.9	-6.90	20.3	9.5	5.4
TAL.21	20	7.2	740	555	268	48.8	0.2	121.8	63.5	44.0	3.2	8.9	12.3	94.4	-32.3	-6.29	18.0	9.3	6.0
TAL.22	19	7.4	1060	795	256	82.2	0.5	115.3	106.2	82.6	0.3	10.9	14.7	118.5	-30.8	-5.75	15.2	14.3	8.5
TAL.23	18	7.4	1040	780	342	72.0	0.5	141.9	112.8	73.6	b.d.l	10.2	16.4	125.2	-33.7	-6.56	18.8	12.2	7.7
TAL.24	19	7.3	640	480	305	37.3	0.2	58.3	39.1	32.6	0.5	10.2	7.7	96.5	-35.0	-6.16	14.2	10.2	1.4
TAL.25	19	7.3	970	728	305	60.8	0.4	115.3	55.0	61.2	0.7	12.4	12.43	124.1	-32.8	-6.14	16.3	15.5	7.8
TAL.26*	25	7.6	1700 [3]	1275 [2]	244	507.2	2.1	5.9	108.2	283.7	1.1	12.8	41.7	67.9	-27.5	-5.19	14.0	-	-
TAL.27*	26	7.7	1900	1425	122	624.9	2.5	6.2	125.7	342.6	0.9	1.4	5.9	69.6	-26.8	-5.13	14.2	12.8	8.7
TAL.28*	28	7.5	3653 [3]	2740 [2]	122	1303.8	4.4	18.7	224.6	871.7	b.d.l	32.1	87.6	73.2	-24.4	-4.45	11.2	-	-
TAL.29*	29	8.6	5832 [3]	4374 [2]	439	2127.5	7.5	9.4	383.8	1168.9	3.6	38.8	106.3	88.1	-22.3	-4.13	10.7	13.9	6.3
TAL.30	20	7.4	730	548	366	42.9	0.2	70.6	54.8	42.3	3.9	12.9	11.7	103.4	-31.8	-6.05	16.7	10.9	4.8
TAL.31	20	7.3	1080	810	366	79.2	0.5	165.8	103.7	82.3	b.d.l	18.1	18.2	120.2	-31.6	-5.92	15.8	10.7	6.1
TAL32*	27	8	18234[3]	36467 [2]	244	20015.9	76.3	0.0	2706.4	11538.5	b.d.l	402.1	1210.9	273.0	4.1	0.23	2.3	6.4[4]	8.8[4]

1: TDS has been determined as TDS = *k*.EC with a correlation coefficient *k* of 0.75 (Rusydi, 2018)

2: TDS has been determined as the sum of major element concentrations

3: EC has been determined as EC = TDS/*k* with a correlation coefficient *k* of 0.75, except for the Mediterranean Sea sample (#32) with *k* = 0.7 (Rusydi, 2018)

4: For stable isotopes of nitrate, this sample of Mediterranean Sea was collected on November 15th, 2019

*: Surface water sample

b.d.l: below detection limit

Table 2. Correlation coefficients between chemical elements

	EC	HCO_3^-	Cl^-	Br^-	NO_3^-	SO_4^{2-}	Na^+	NH_4^+	K^+	Mg^{2+}	Ca^{2+}	pH	$\delta^{15}N$
EC	1												
HCO_3^-	0.36	1											
Cl^-	**0.72**	0.17	1										
Br^-	**0.79**	0.21	**0.95**	1									
NO_3^-	0.03	0.10	0.12	0.15	1								
SO_4^{2-}	0.12	0.01	0.03	0.02	0.19	1							
Na^+	**0.84**	0.40	**0.73**	**0.72**	0.04	0.04	1						
NH_4^+	0.02	0.10	0.04	0.03	0.01	0.03	0.07	1					
K^+	0.01	0.03	0.03	0.03	0.41	0.05	0.02	0.05	1				
Mg^{2+}	**0.58**	**0.53**	**0.60**	**0.62**	0.12	0.01	**0.60**	0.06	0.02	1			
Ca^{2+}	0.28	0.43	0.05	0.09	0.01	0.12	0.10	0.01	0.05	0.31	1		
pH	0.01	0.13	0.01	0.01	0.04	0.01	0.03	0.01	0.2	0.01	0.07	1	
$\delta^{15}N$	0.4	0.02	0.3	0.4	0.03	0.08	0.3	0.01	0.02	0.2	0.1	0.04	1

Bold characters show a significant correlation

Table 3. Calculated coefficient of variation (CV) from hydrogeochemical data

	Cl^-	Br^-	Na^+	Mg^{2+}
Max	361.27	1.81	237.56	49.32
Min	37.25	0.22	32.61	7.73
Ave	103.06	0.58	72.41	19.44
SD	74.90	0.39	42.30	9.30
CV (%)	73	68	58	48

4.2 **Hydrogeochemical characterization**

4.2.1 Groundwater chemical compound analysis

Table 1 indicates that groundwater chemical analyses reveal acceptable concentrations in SO_4^{2-} compared to the drinking water limit of 500 mg/L suggested by the World Health Organization (WHO, 2017). Excessive groundwater concentrations are revealed for NH_4^+ for 26% of groundwater samples, with a maximum of 3.9 mg/L and a median of 0.3 mg/L, relative to the maximum permissible limit of 0.5 mg/L. High concentrations were obtained for Cl^- with a maximum of 361.3 mg/L and a median of 72 mg/L. Excessive levels were also recorded for HCO_3^- (671 mg/L; median of 366 mg/L), Na^+ (237.6 mg/L; median of 70.3 mg/L), Br^- (1.8 mg/L; median of 0.5 mg/L), and K^+ (18.1

mg/L; median of 6.6 mg/L). The groundwater was slightly alkaline with pH values ranging from 7 to 7.5 with no significant spatial variation. The groundwater EC values were seen to range from 510 µS/cm to 1870 µS/cm; the higher values (>1,000 µS/cm) were recorded at the borders of the study area.

According to Table 2, Cl^- is significantly correlated with Na^+ (R^2 = 0.73), suggesting that they probably have the same origin. In Figure 6a, the continuous equivalent or parallel increase between Na^++K^+ and Cl^-+SO_4^{2-} suggests a geogenic origin of these ions (Meybeck, 1987). However, the concentrations of these elements do not fall along the equiline of 1:1 for all groundwater samples, suggesting that Na^+ and Cl^- chemistry are affected by more than one process. In Figure 6b, high Cl^- concentrations (above the equiline of 1:1) are mostly observed for the groundwater samples collected from wells located along the Guebli River, suggesting a possible influence of water enriched in Cl^- from the Guebli river. Conversely, certain groundwater samples in Figure 6b show a slight dominance of Na^+ (below the equiline of 1:1). When classic precipitation water (Ca-HCO_3 in composition) infiltrates granular deposits, Ca^{2+} can be taken up from the freshwater to replace Na^+, which is released from the cation exchanger in the groundwater. This process contributes Na^+ to groundwater, and is known to occur in coastal aquifers (Appelo and Postma, 2005; Walter et al., 2017). The absence of a significant change between the trend of Na^+ versus Cl^- (Figure 6b) and that of Na^++K^+ versus Cl^- (Figure 6c) indicates a slight contribution of K^+, probably due to slower weathering rates of potassium-bearing minerals (Huang et al., 2016). A good correlation is observed between Br^- and Cl^- (R^2=0.95), as well as between Br^- and Na^+ (R^2=0.72). Br^- is commonly found in nature along with Cl^- and Na^+, owing to their similar physical and

chemical properties, but in smaller quantities (WHO, 2017). A moderate correlation is observed between Mg^{2+} and Cl^- (R^2=0.60), thus involving a moderate correlation between Mg^{2+} and Br^- (R^2=0.62), given the good correlation between Cl^- and Br^- (Table 2). Generally, the increase of Ca^{2+}+Mg^{2+} with increasing Cl^- concentrations (Figure 6d) may be due in part to reverse ion exchange (Jankowski et al., 1998). However, the moderate correlation between Mg^{2+} and Cl^- corresponds approximately to an equiline of 1:4 (Figure 6e), indicating that Cl^- is approximately 4 times more abundant than Mg^{2+}. Consequently, Cl^- has another contributing source. When Mg^{2+} is plotted as a function of Na^+, a moderate correlation is found (R^2=0.60, Table 2), but all concentrations fall above the equiline of 1:1 (Figure 6f), suggesting that Na^+ potentially has another contributing source. The other contribution sources for both Na^+ and Cl^- (Figure 6e and 6f) suggest a potential influence of seawater intrusion, as the study area is a coastal aquifer. Table 2 indicates that Mg^{2+} is in moderate correlation with HCO_3^- (R^2 = 0.53); and the examination of Figure 6j, combining Ca^{2+}+Mg^{2+} and HCO_3^-+ SO_4^{2-} contents, suggests that dissolution of carbonate formation exerted some control on Ca^{2+}, Mg^{2+}, SO_4^{2-}, and HCO_3^- contents (Drever, 1988; Huang et al., 2016; Rajmohan and Elango, 2004). However, both Mg^{2+} and HCO_3^- can also be traced back to anthropogenic activities (Bouzourra et al., 2015). The plotting of HCO_3^- versus Mg^{2+} in Figure 6h shows that all concentrations fall above the equiline of 1:1. This observation indicates that HCO_3^- is more abundant than Mg^{2+}. Meteoritic water (Ca-HCO_3 in composition) could also contribute to HCO_3^- in groundwater (Hiscock, 2009).

The mineral saturation indices of the collected groundwater samples are calculated using the hydrogeochemical program PHREEQC (Parkhurst and Appelo,

1999). A saturation index value less than zero refers to a dissolution state, while a saturation index value greater than zero refers to a precipitation state (Appelo and Postma, 2005). The main minerals which are considered in the aquifer are calcite, gypsum and halite (Beloulou, 1987; Boulabeiz, 2006). Dolomite is also considered to predict the origin of Mg^{2+}. Table 4 presents the calculated saturation indices for the considered minerals. The saturation indices of calcite show that 78% of the groundwater samples are oversaturated (saturation index >0) suggesting, as previously mentioned above, the main contribution of potential precipitation water (Ca-HCO_3 in composition). The saturation indices of dolomite show that 93% of the groundwater samples are under-saturated (saturation index <0), while those of gypsum and halite show that all groundwater samples are under-saturated. The under-saturation by dolomite (Ca-Mg dominant), gypsum (Ca-SO_4 dominant) and halite (Na-Cl dominant) suggest a geogenic origin of the elements Na^+, Cl^-, Mg^{2+} and SO_4^{2-} via a dissolution process, as previously mentioned above. The correlation between the saturation indices of the considered minerals is poor ($R^2 \leq 0.1$), except for the correlation between the saturation indices of calcite and those of dolomite ($R^2 = 9.4$) which indicate that gypsum and/or halite dissolution does not considerably contribute to groundwater calcium content (Argamasilla et al., 2017; Gilabert-Alarcón et al., 2018). Thus, as previously mentioned above, a removal of Ca^{2+} and Mg^{2+} may occur by means of other processes such as reverse cation-exchange reactions and precipitation.

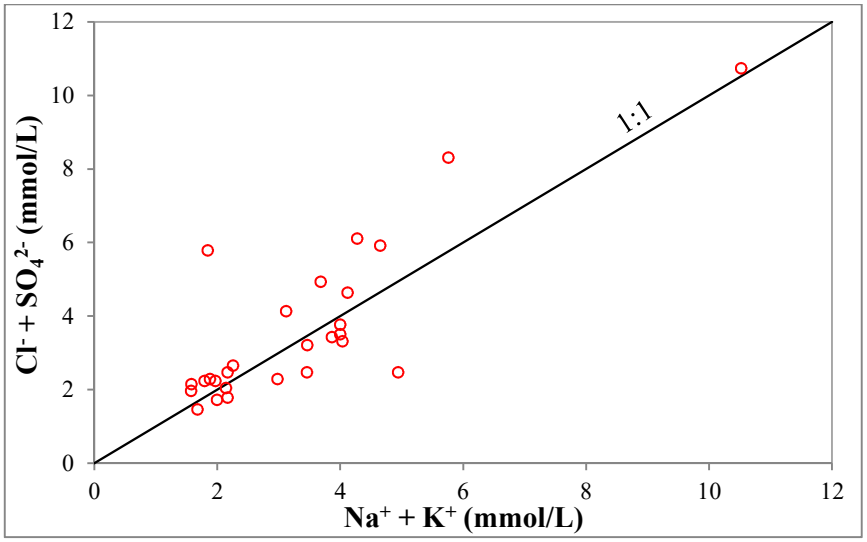
Cl⁻ + SO4²⁻ (mmol/L)
Na⁺ + K⁺ (mmol/L)
1:1
0
2
4
6
8
10
12

(a)

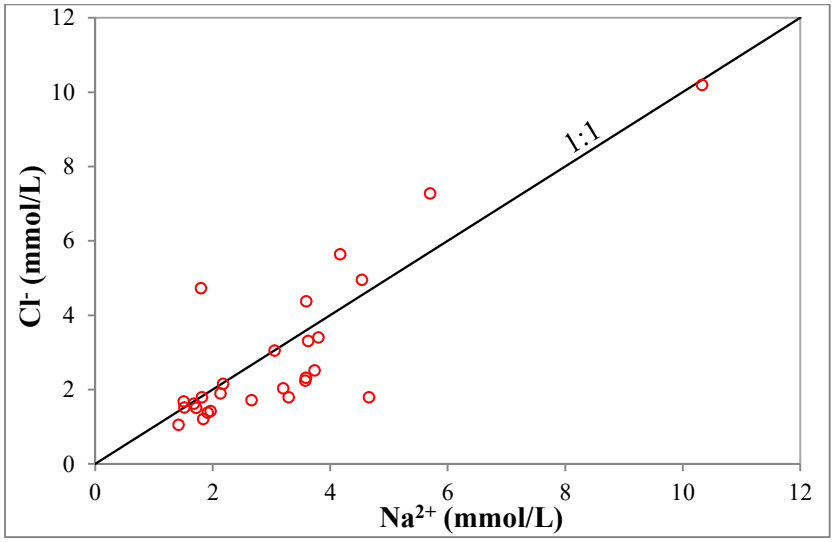
Cl⁻ (mmol/L)
Na²⁺ (mmol/L)
1:1
0
2
4
6
8
10
12

(b)

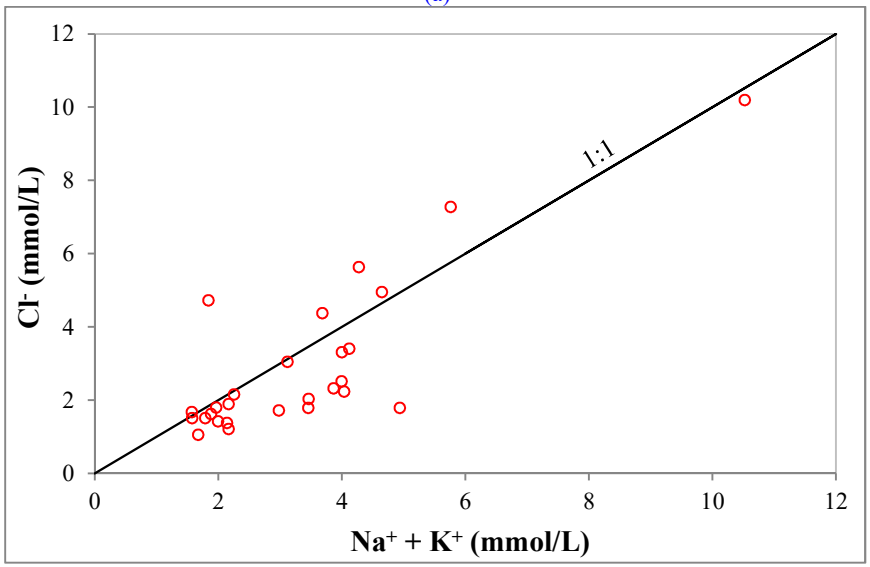
Cl⁻ (mmol/L)
Na⁺ + K⁺ (mmol/L)
1:1
0
2
4
6
8
10
12

(c)

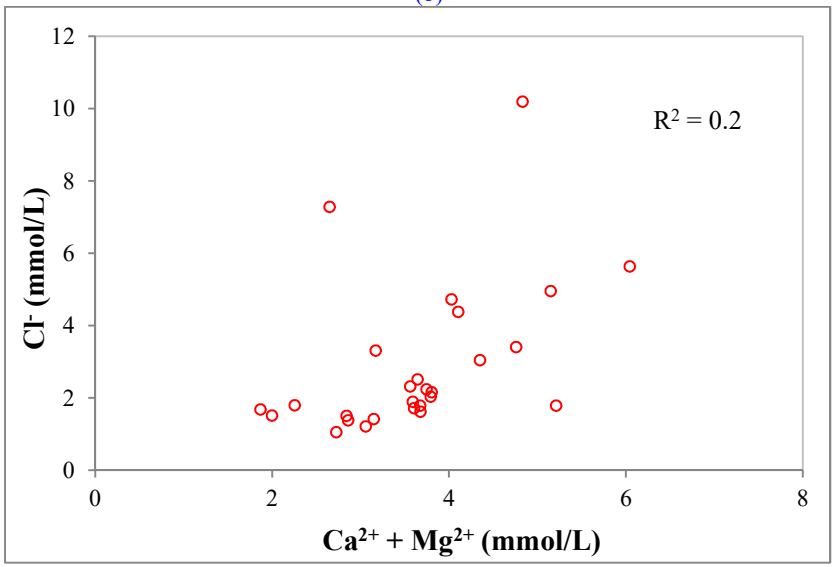
Cl⁻ (mmol/L)
Ca²⁺ + Mg²⁺ (mmol/L)
R² = 0.2
0
2
4
6
8
10
12

(d)

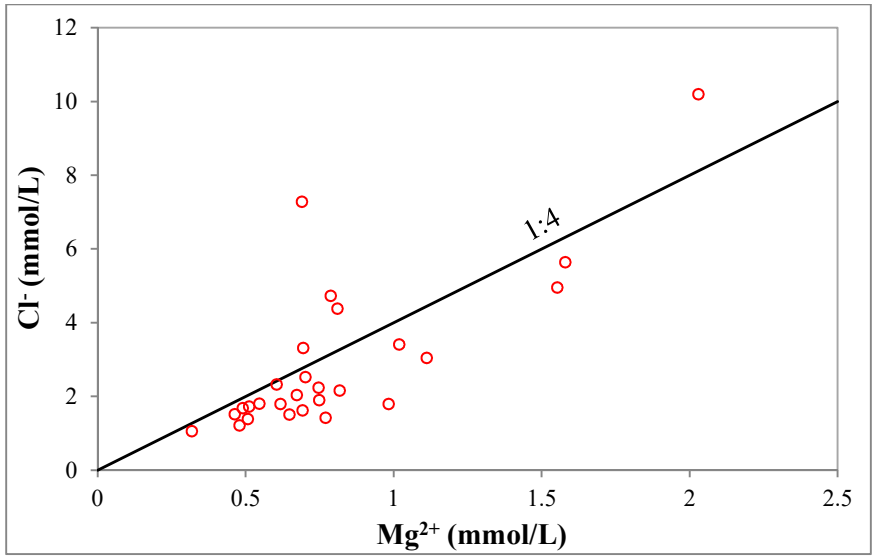
Cl- (mmol/L)
Mg2+ (mmol/L)
1:4
0
2
4
6
8
10
12
0
0.5
1
1.5
2
2.5

(e)

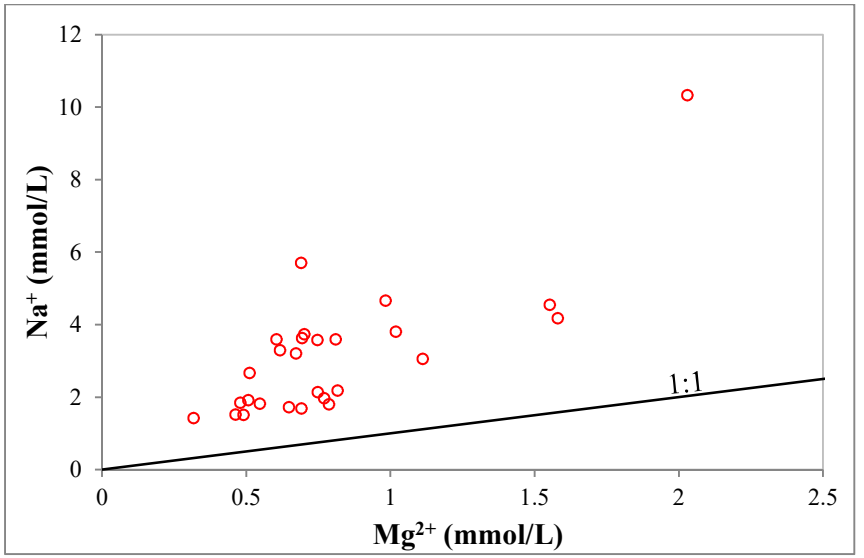
Na+ (mmol/L)
Mg2+ (mmol/L)
1:1
0
2
4
6
8
10
12
0
0.5
1
1.5
2
2.5

(f)

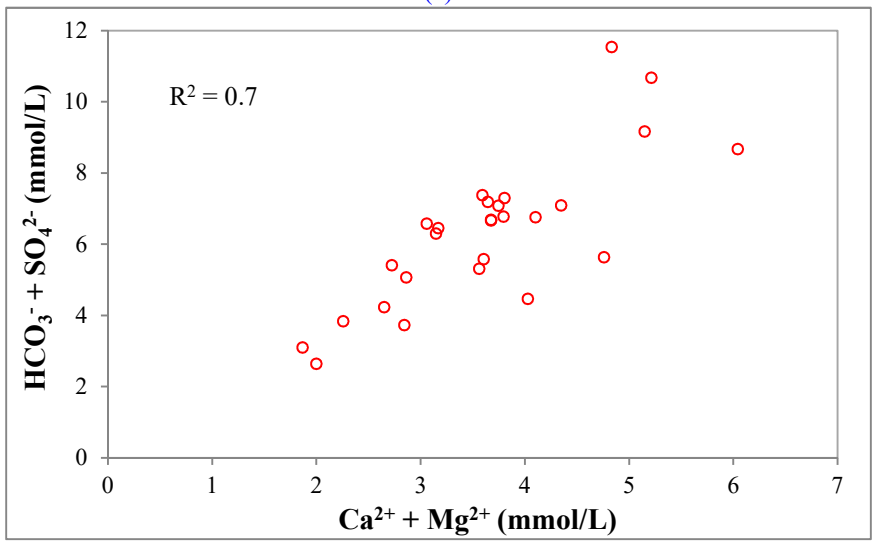
HCO3- + SO4 2- (mmol/L)
Ca2+ + Mg2+ (mmol/L)
R2 = 0.7
0
2
4
6
8
10
12
0
1
2
3
4
5
6
7

(j)

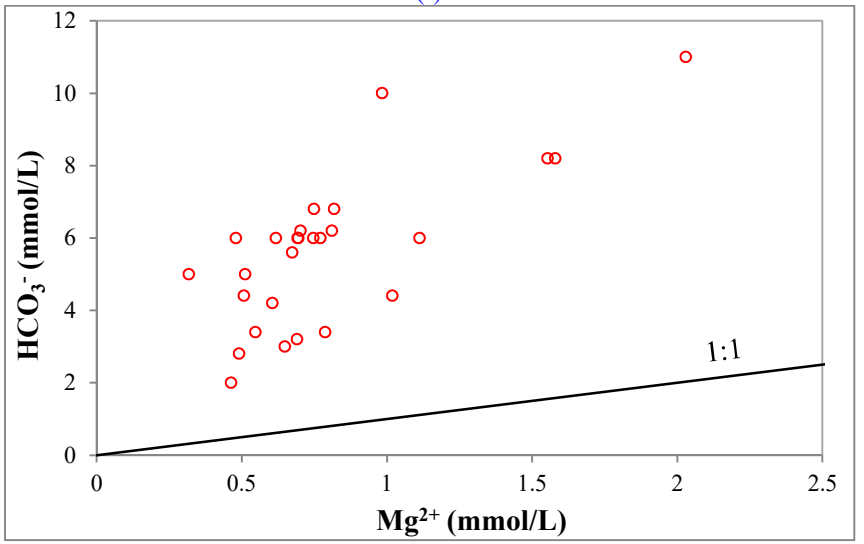
HCO3- (mmol/L)
Mg2+ (mmol/L)
1:1
0
2
4
6
8
10
12
0
0.5
1
1.5
2
2.5

(h)

Figure 6. (a) continuous increase between $Na^{+}+K^{+}$ and $Cl^{-}+SO_4^{2-}$; (b) relationship between Na^{+} and Cl^{-} concentrations; (c) continuous increase between $Na^{+}+K^{+}$ and Cl^{-}; (d) relationship between $Ca^{2+}+Mg^{2+}$ and Cl^{-} concentrations; (e) relationship between Mg^{2+} and Cl^{-} concentrations; (f) relationship between Mg^{2+} and Na^{+} concentrations; (j) continuous increase between $Ca^{2+}+Mg^{2+}$ and $HCO_3^{-}+SO_4^{2-}$; (h) relationship between Mg^{2+} and HCO_3^{-}.

Table 4. Saturation indices of groundwater samples collected from the study area.

	Saturation index (Log IAP/KT)[1]			
Groundwater sample	Calcite	Dolomite	Gypsum	Halite
TAL-1	0.59	0.55	-1.9	-5.68
TAL-2	-0.1	-1.20	-1.98	-7.14
TAL-3	0.44	-0.23	-1.73	-7.06
TAL-4	0.41	-0.11	-1.74	-6.33
TAL-5	0.39	-0.28	-1.78	-7.0
TAL-6	0.13	-0.84	-1.44	-6.75
TAL-7	-0.03	-1.06	-2.06	-7.22
TAL-8	-0.17	-1.37	-1.69	-6.43
TAL-9	-0.55	-2.06	-2.21	-7.25
TAL-10	0.36	-0.40	-1.72	-6.48
TAL-11	0.44	-0.31	-1.64	-6.90
TAL-12	0.23	-0.52	-1.45	-6.71
TAL-13	-0.34	-1.65	-1.64	-6.06
TAL-14	0.36	-0.34	-1.89	-6.60
TAL-15	0.18	-0.70	-1.36	-6.58
TAL-16	0.88	0.67	-1.59	-6.77
TAL-17	0.31	-0.52	-1.51	-6.7
TAL-18	0.33	-0.17	-1.51	-6.34
TAL-19	0.34	-0.46	-1.65	-7.24
TAL-20	-0.45	-1.91	-1.84	-7.29
TAL-21	0.02	-1.12	-1.71	-7.24
TAL-22	0.25	-0.71	-1.45	-6.75
TAL-23	0.37	-0.46	-1.41	-6.86
TAL-24	0.19	-1.03	-1.89	-7.49
TAL-25	0.27	-0.77	-1.69	-7.01
TAL-30	0.39	-0.46	-1.75	-7.32
TAL-31	0.31	-0.48	-1.47	-6.78

1: IAP is the ion activity product of the dissociated chemical species in solution, and KT is the equilibrium solubility product for the chemical involved at the sample temperature.

4.2.2 Sources and fate of nitrate in groundwater

Groundwater nitrate concentrations range from 1.6 to 235 mg/L, with a median value of 68.5 mg/L (Table 1). For 96% of the groundwater samples, the nitrate concentration exceeds, the natural baseline threshold value of 5 to 7 mg/L (Appelo and Postma, 2005; Panno et al., 2006), and exceeds the drinking water limit of 50 mg/L (WHO, 2017) for

about 70% of groundwater samples. Figure 7 shows that in the current study area, the groundwater samples featuring moderate concentrations (5 mg/L < NO_3^- < 40 mg/L) are located in its southern and southeastern sector. These groundwater samples are perfectly grouped and consistently similar, except groundwater sample #6 which presents a high concentration of nitrate (70 mg/L). This particular observation was also revealed in the same location during the 2005 groundwater campaign (Boulabeiz, 2006), during which a nitrate concentration of 75 mg/L was recorded (the potential source of nitrate is still active in this location). This groundwater sampling sector, which revealed moderate concentrations in 2019 (NO_3^- ranging from 5 to 40 mg/L – Figure 7), was identified in 2005 as having lower concentrations ranging from 1.5 to 4.5 mg/L (Boulabeiz, 2006). In this sector, the increase in nitrate concentration over 14 years (2005-2019) seems to originate from a continuous and developing source. Further northwards to the northwestern parts of the study area, the groundwater samples show high concentrations in nitrate (Figure 7). During the 2005 campaign, these sectors revealed high concentrations in nitrate (Boulabeiz, 2006). At that time the maximum level observed was 140 mg/L, whereas it reached 235 mg/L in the present study. It seems quite probable that in those sectors, the increase in nitrate concentration over 14 years (2005-2019) seems to originate from a continuous and developing source.

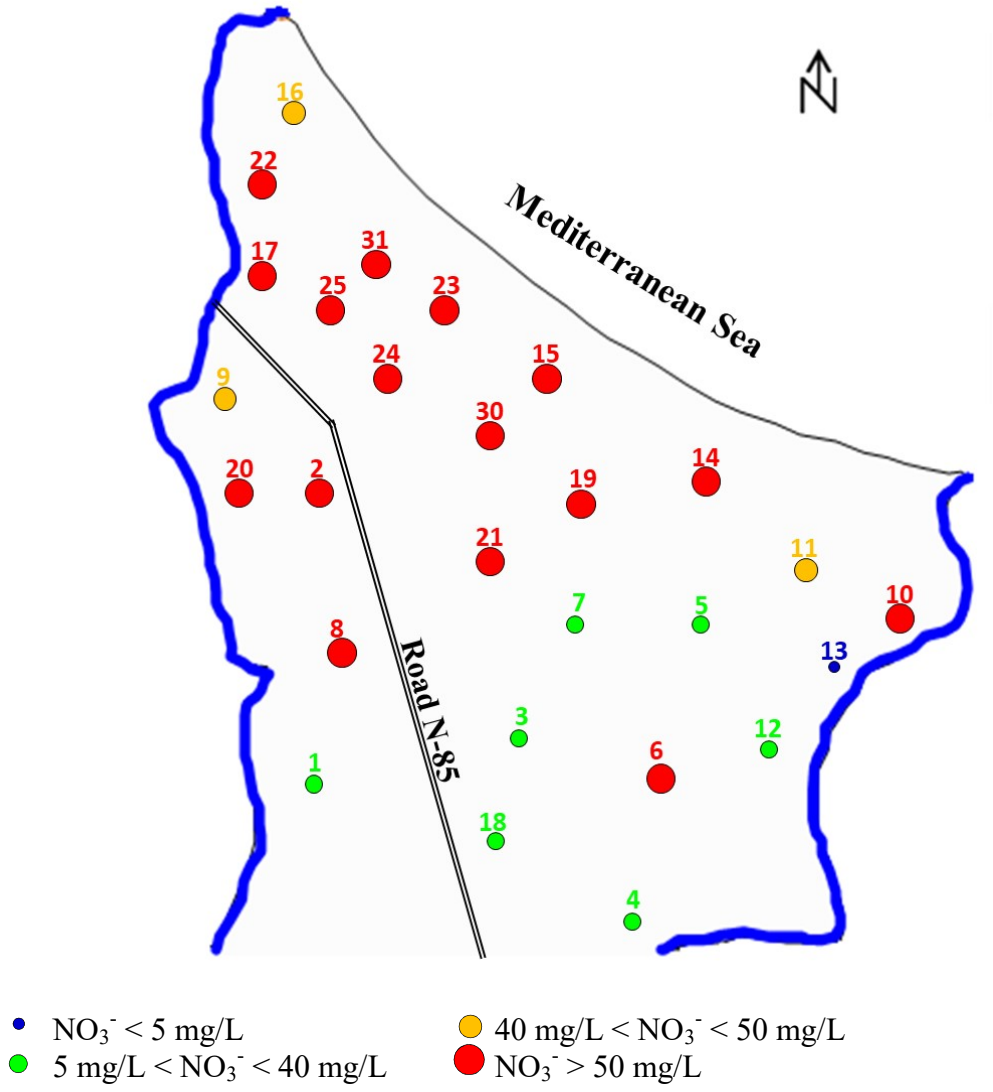

Figure 7. Spatial distribution of NO3- concentrations over the study area.

The groundwater δ^{15}N-NO_3 values range from 2‰ to 19.9‰ (*n*=26), with a median value of 11‰; and the measured δ^{18}O-NO_3 values range between 1.4‰ and 12.7‰ (*n*=26), with a median value of 5.7‰ (Table 1). The values of δ^{15}N-NO_3 and δ^{18}O-NO_3 in the water surface sample TAL-27 collected from the Guebli River are 12.8‰ and 8.7‰, respectively; in the water surface sample TAL-29 collected from Cherka River the values are 13.9‰ and 6.3‰. The Mediterranean Sea sample (TAL-32) presents values of 6.4‰

and 8.8‰ for $\delta^{15}N\text{-}NO_3$ and $\delta^{18}O\text{-}NO_3$, respectively. Nitrate source identification based on stable isotopes was carried out by comparing the concentrations of $\delta^{15}N\text{-}NO_3$ and $\delta^{18}O\text{-}NO_3$ with those expected for the different types of nitrate sources. Kendall's diagram (Kendall, 1998), commonly used in the literature to identify nitrate sources, is used for this purpose (Figure 8). All water samples indicate manure and human septic waste as the main source of nitrate, with the exception of two groundwater samples (TAL-3 and TAL-8) and the sample collected from the Mediterranean Sea (TAL-32), whose isotopic ratios plot in the overlapping area of different sources: nitrate from manure and septic waste, soil-derived nitrogen, and nitrate formed from nitrification of ammonium in mineral fertilisers or rain.

Compared to other studies conducted in urban areas (Fukada et al., 2004; Zendehbad et al., 2019), and despite differences in study area conditions, the signatures of $\delta^{15}N\text{-}NO_3$ and $\delta^{18}O\text{-}NO_3$ in the present study are relatively similar. Consequently, they suggest a sewage-derived source for nitrate. This finding agrees with the land occupation profile of the Taleza plain (Figure 3): the high nitrate concentrations (>50 mg/L, Figure 7) were observed in the sectors mostly occupied by higher population densities. This population uses inadequate private sanitation systems that deliver an important quantity of nitrates to the aquifer, as the public sanitation network is not yet functional.

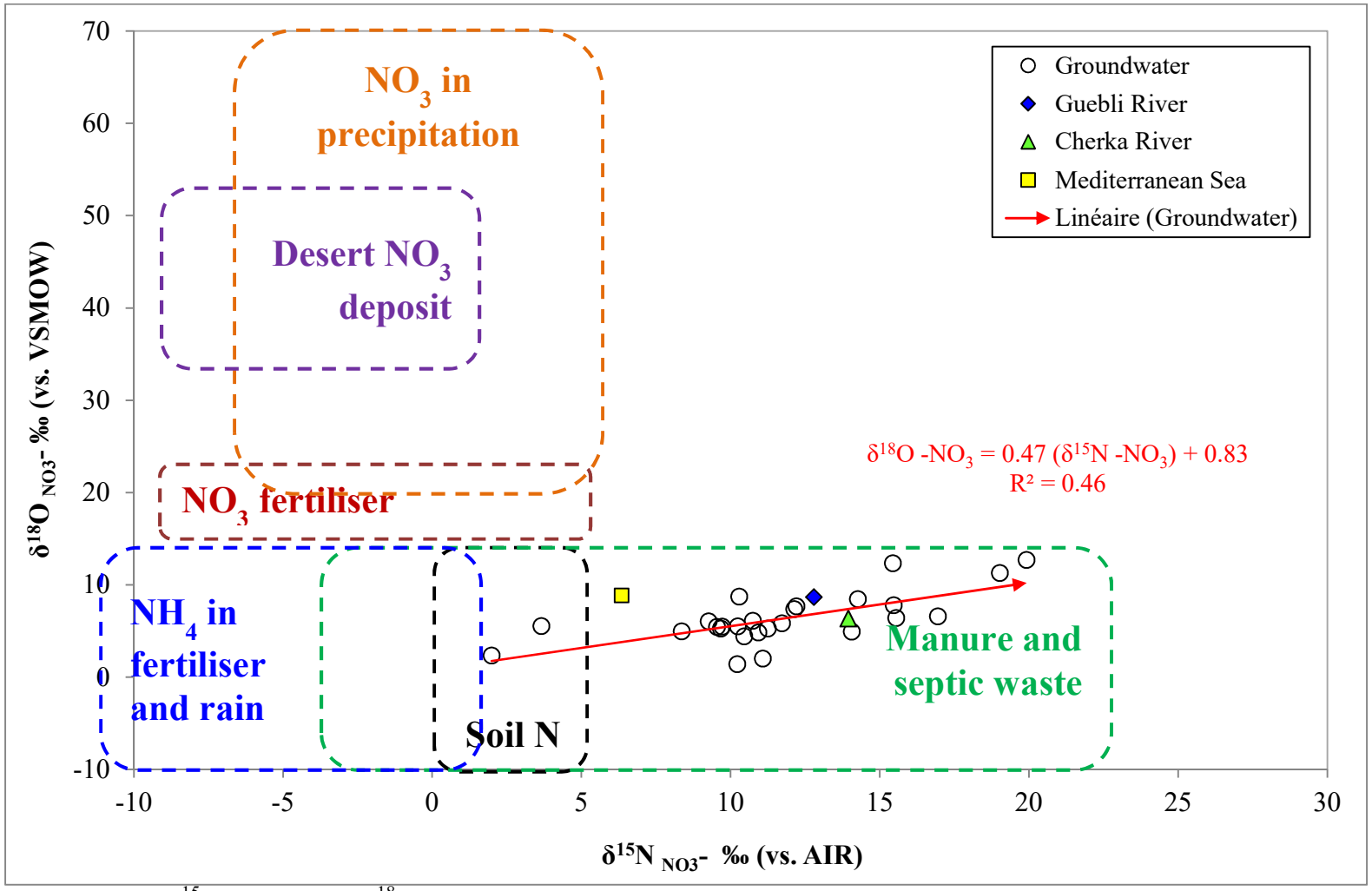

Figure 8. Plot of δ^{15}N-NO_3 versus δ^{18}O-NO_3 values of nitrate in the groundwater and surface water of the study area shown in a Kendall's diagram (modified from Kendall (1998)).

In many countries, a recommended practice is to use a septic tank combined with a seepage field (e.g. MDDELCC, 2015). In the expanding urban area of Taleza, however, home owners have built open-bottom sewage storage systems through which wastewater can directly seep into the ground, causing groundwater contamination (Boumaiza et al., 2019b). Sulfides (H_2S) can be produced during the anaerobic degradation of organic substances present in septic tanks (Gujer and Zehnder, 1983), and can generate a toxic gas that smells like rotten eggs. This odor has been identified for groundwater pumped from certain private wells (Boumaiza et al., 2019a) in the study area. Even though nitrate isotopes do not make it possible to distinguish manure-derived nitrate from sewage-derived nitrate, since these two sources of nitrate have overlapping isotopic signatures (Aravena and Mayer, 2009; Kendall et al., 2007), it can be stated that the high nitrate concentrations observed in the southeastern sector of the study area (Figure 7) are mostly explained by (i) excessive manure produced by a number of animal farms present in this sector (Figure 7) and/or (ii) excessive amounts of manure used to fertilise the agricultural areas (Boumaiza et al., 2019b). As can be seen in Figure 3, except for the southwestern area which is dominated by seasonal cereal production, the rest of the agricultural areas are dominated by the production of legumes. This culture is practiced during the entire year in open agricultural fields as well as under plastic greenhouses. Since the 1990s, the use of industrial synthetic fertilizers was prohibited by the Algerian Government, as these products have been used in other illegal activities rather than agriculture (Chabour, 2004). Consequently, animal manures have been intensively used to fertilise agricultural areas. Although the concentration of nitrate in the Mediterranean Sea sample (TAL-32) was 0 mg/L (sample collected in June 2019 - Table 1), isotopic ratios of nitrate have been

revealed in this sample ($\delta^{15}N\text{-}NO_3$ = 6.4 ‰ and $\delta^{18}O\text{-}NO_3$ = 8.8 ‰ - Table 1). The Mediterranean Sea sample obtained for analysis of the stable isotope of nitrate was collected in November 2019 (for logistical reasons). In November 2019 (rainy season), the rivers bordering the Taleza aquifer were very active, contributing greater inputs containing organic contamination to the Mediterranean Sea, compared to the June 2019 (dry season), where there is less interaction between the rivers and the Mediterranean Sea (which is why there was a nitrate concentration of 0 mg/L). As the Mediterranean Sea isotopic nitrate ratios indicate sewage-derived sources, this finding confirms the contamination of Mediterranean Sea by the two bordering rivers.

The combined analysis of $\delta^{15}N\text{-}NO_3$ and $\delta^{18}O\text{-}NO_3$ makes it possible to evaluate nitrate transformation processes in a groundwater system subjected to microbial denitrification, since $\delta^{15}N\text{-}NO_3$ and $\delta^{18}O\text{-}NO_3$ values increase during denitrification, while nitrate concentrations are reduced (Böttcher et al., 1990; Wassenaar, 1995). The denitrification process in groundwater is traced by observing a positive linear relationship between $\delta^{15}N\text{-}NO_3$ and $\delta^{18}O\text{-}NO_3$ in an equiline of 2:1 (Aravena and Robertson, 1998; Mengis et al., 1999; Singleton et al., 2007). The combined use of $\delta^{15}N\text{-}NO_3$ and $\delta^{18}O\text{-}NO_3$ in Figure 8 shows a non-linear relationship between $\delta^{15}N\text{-}NO_3$ and $\delta^{18}O\text{-}NO_3$ given the moderate correlation coefficient of 0.46. The slightly pronounced trend of $^{15}N\text{-}NO_3$ versus $\delta^{18}O\text{-}NO_3$ also suggests a moderate denitrification process. However, it is difficult to distinguish between mixing of differently denitrified sources and actual denitrification. During the denitrification process, the $\delta^{15}N\text{-}NO_3$ is retained in the remaining nitrate (Kendall et al., 2007; Mayer, 2005). Thus, the $\delta^{15}N\text{-}NO_3$ values of the remaining nitrate increase as the nitrate concentration decreases. This finding is not observed in Table 2 which presents a poor correlation between $\delta^{15}N\text{-}NO_3^-$ ratios and NO_3^- concentrations.

Moreover, evidence of denitrification as the microbial reduction of nitrate may induce an increase in pH (Rivett et al., 2008; Rust et al., 2000). Such an observation has not been found, given the weak correlation between NO_3^- concentrations and groundwater pH (Table 2).

4.3 **Saltwater intrusion**

The piezometric map (Figure 9), based on groundwater level measurements (the low-water period of June 2019) obtained at private wells investigated in the study area, shows that groundwater flow is oriented towards both the Mediterranean Sea and the bordering rivers. Inverse groundwater flow from the bordering rivers towards the aquifer, via upstream migration of seawater through the river mouths, is expected during the high-water period; this has already been identified by Boulabeiz (2006). Evidence of saltwater influence is identified (section 4.3.1) and further confirmed by the three methods used in this study for evaluating saltwater intrusion (section 4.3.2).

4.3.1 Evidence of saltwater influence

The δ^2H-H_2O and $\delta^{18}O$-H_2O values for the samples drawn from groundwater, the two rivers and the Mediterranean Sea are listed in Table 1 and shown in Figure 10. The isotopic ratios of groundwater range from -7.4‰ to -5.75‰ with a median value of -6.16‰ for $\delta^{18}O$; and from -35.7‰ to -30.8‰ with a median value of -33.3‰ for δ^2H. All groundwater samples plot in the expected value range of LMMWL, which is indicated in Figure 10 by its upper and lower limits both derived from d-excess values, ranging from 14‰ to 27‰, proposed by Gat et al. (2003) for the Mediterranean area closest to the study area. Despite the wide range of meteoric water origin shown in Figure

10, there is a clear indication of isotope enrichment towards a mixing with Mediterranean Seawater.

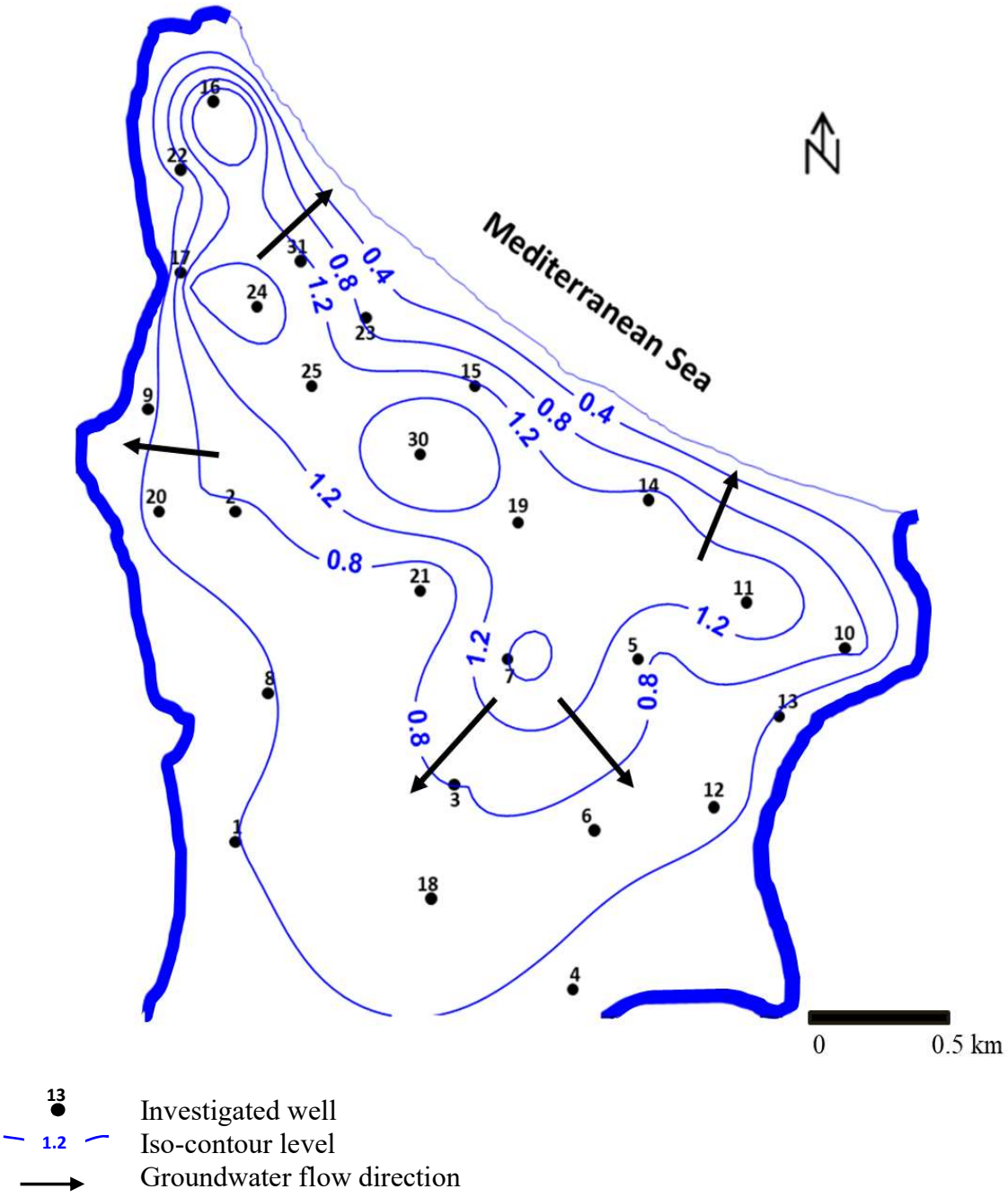

Figure 9. June 2019 piezometric contours and locations of the investigated wells (this piezometric map is traced using SURFER; the iso-contour levels are interpolated using the Kriging approach).

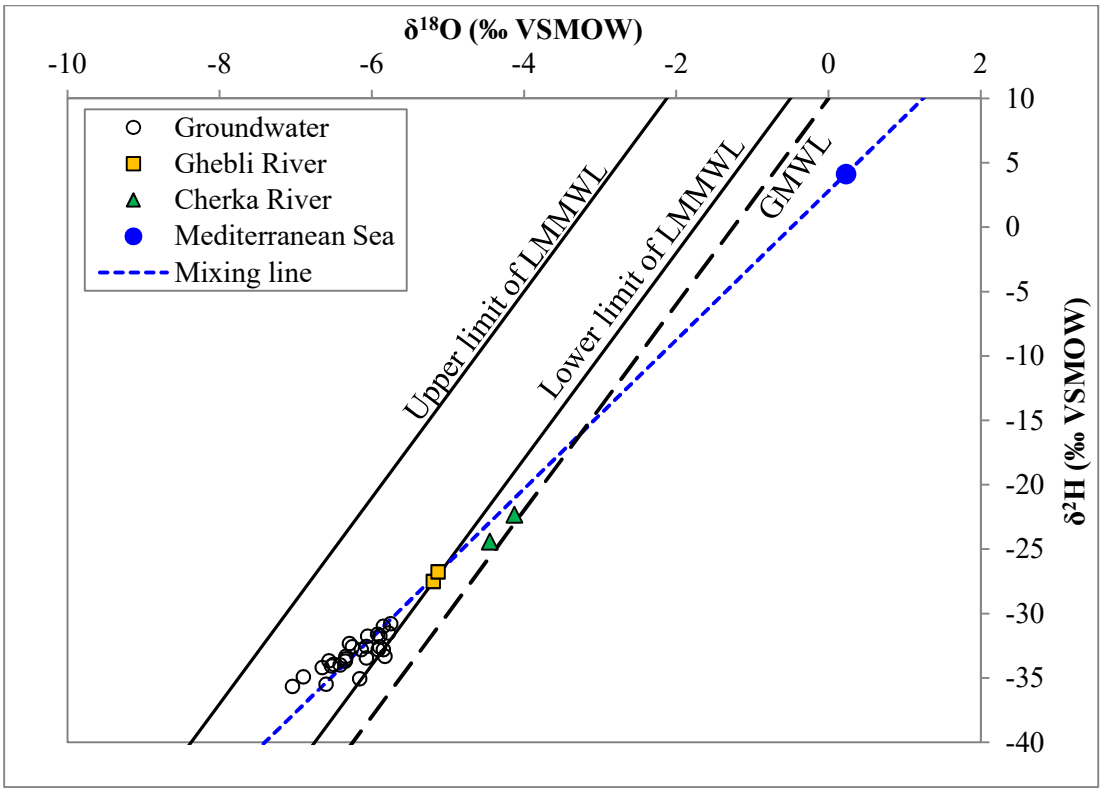

Figure 10. Distribution of isotopic ratios of the collected water samples. The upper and lower limits of LMMWL are derived from d-excess values proposed by Gat et al. (2003).

The Guebli River surface water samples display heavier water isotope values (from -4.45‰ to -4.13‰ for $\delta^{18}O$, and from -24.4‰ to -22.3‰ for $\delta^{2}H$) compared to those of groundwater samples. Similarly, the two surface water samples collected from the Cherka River are also more enriched in heavy isotopes compared to groundwater. This enrichment in heavy isotopes is typical for water that has been subjected to open surface evaporation such as in rivers or for water that is mixed with seawater (Dindane et al., 2003), but as the surface water samples plot above the Global Meteoric Water Line (Craig 1961), mixing with seawater is expected. This is in agreement with the surface water flow because the Cherka River, which drains a smaller watershed, exhibits a lower flow rate than the Guebli River which drains a large sub-watershed covering an area of 993 km^2 (Mecibah, 2008). Furthermore, the lower flow rate in the Cherka River could

contribute to more seawater diffusion compared to the Guebli River. In fact, a d-excess median value of 10.9‰ is obtained for the Cherka River surface water samples compared to a median value of 14.1‰ obtained for the Guebli River surface water samples, suggesting that seawater exerts a greater influence on the Cherka River than on the Guebli River. This finding is also supported by a Cl^--$\delta^{18}O$ quasi-linear relationship (Han and Currell, 2018), wherein the contribution of Cl^- from the Mediterranean Sea to the Cherka river is more important than to the Guebli River (Figure 11a). When the Mediterranean Sea becomes turbulent, the diffusion process could potentially occur simultaneously with an advection process. In the Taleza valley, both aquifer and rivers are influenced by seawater. The influence of seawater on the bordering rivers in particular can be argued thanks to the chemical analyses of surface-water samples (TAL-26, 27, 28 and 29) collected from the Guebli and Cherka rivers. In fact, Table 1 shows particularly high concentrations for the common chemical elements (Cl^-, SO_4^{2-}, Na^+, Mg^{2+}, and Br^-) usually characterizing the high salinity of the Mediterranean Sea (sample TAL-32). Potential saltwater intrusion from the two rivers bordering the aquifer is expected during the high-water period. Some researchers have used the correlation between Cl^-/Br^- ratio to Cl^- as a proxy to trace water contamination, whereby the Cl^-/Br^- ratio is determined from concentrations expressed in moles, rather than mg/L (Alcalá and Custodio, 2008; Davis et al., 2004). Figure 11b shows that most groundwater samples collected are located around point 2e, corresponding to coastal contaminated areas (agreeing with study area condition), with a trend towards point 1b, corresponding to seawater intrusion. Accordingly, the seawater intrusion could be proposed as process affecting Cl^-/Br^-.

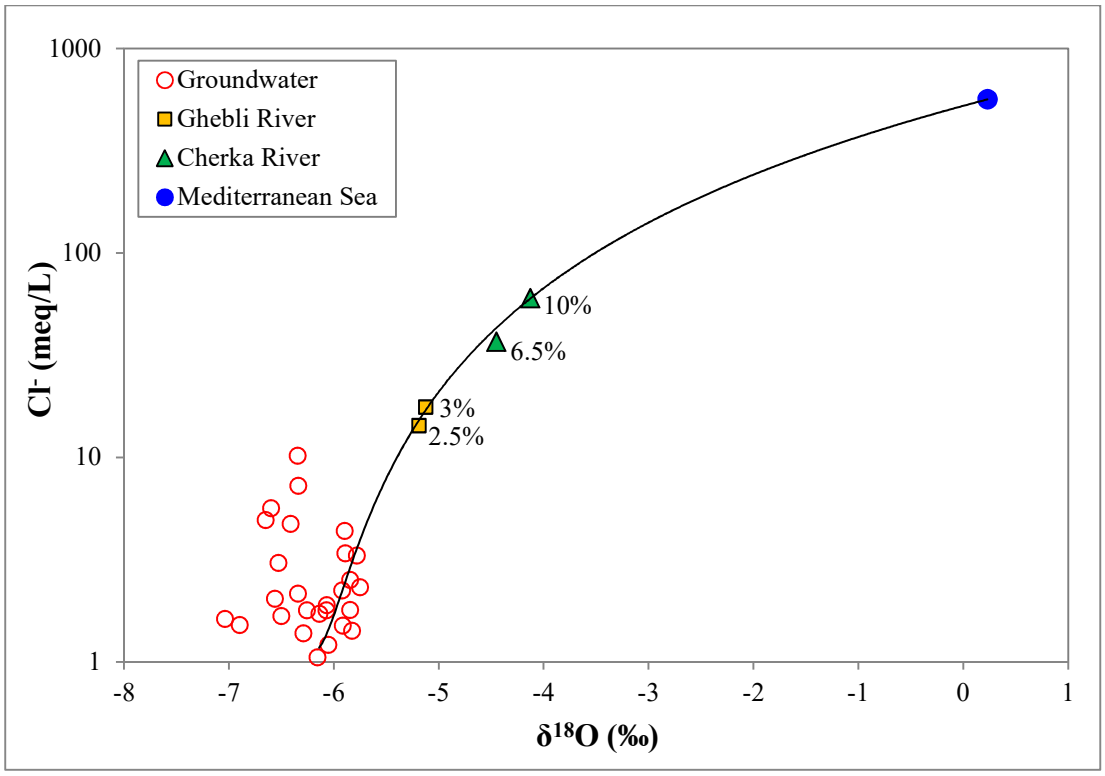

(a)

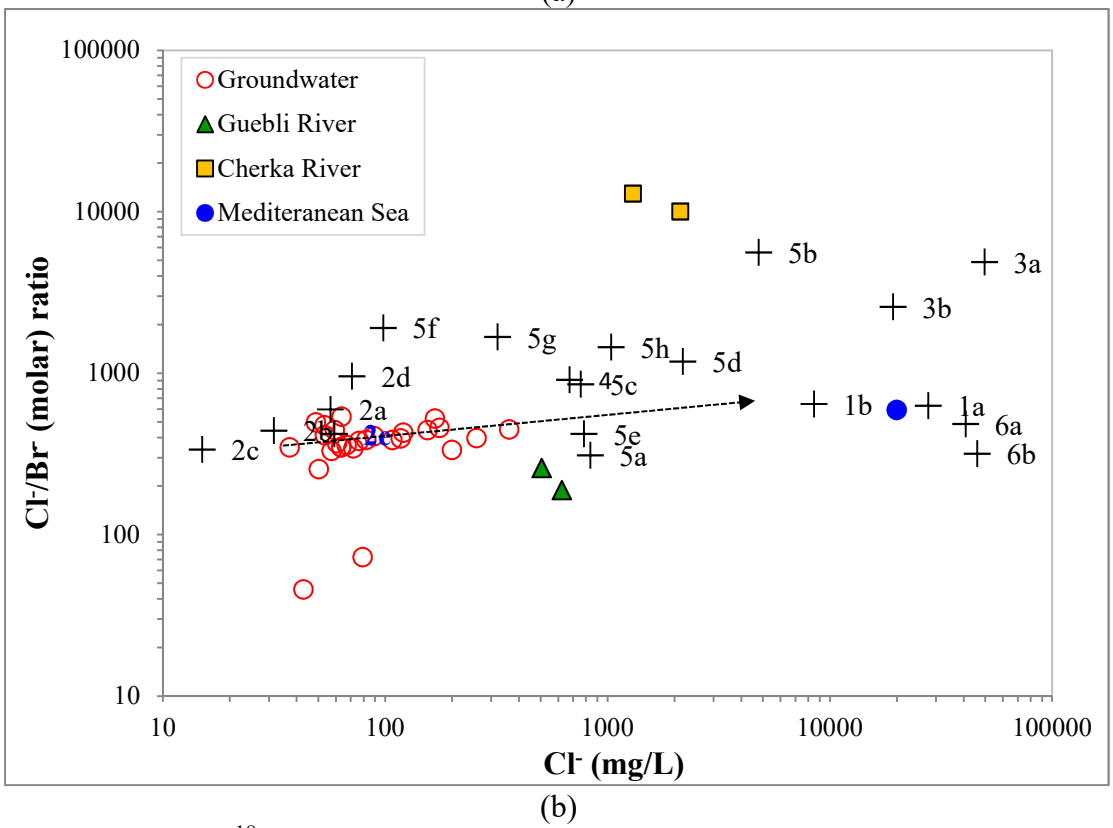

(b)

Figure 11. (a) Cl^--$\delta^{18}O$ relationship with seawater contribution fraction (expressed in %) calculated as Cl^- concentration of the water sample relative to Cl^- concentration of

Mediterranean Sea as suggested by Appelo and Postma (2005); (b) Plotting of water sample concentrations of the Cl^-/Br^- molar ratios versus Cl^- diagram (modified from Alcalá and Custodio (2008). Fields are: 1a: seawater brines; 1b: seawater intrusion; 2a: coastal areas; 2b: inland areas; 2c: high altitude/continental; 2d: coastal arid climate; 2e: coastal contaminated areas; 3a: leaching of natural halite; 3b: leaching of gypsum containing halite; 4: volcanic halides; 5a: agricultural contamination; 5b: leaching of halite (road salt); 5c: leaching of garbage and solid waste; 5d: urban wastewater, 5e: septic waste; 5f: septic-tank outflow; 5g: sewage effluent; 5h: animal waste; 6a: leaching of carnalite; 6b: leaching of sylvite.

4.3.2 Confirming saltwater intrusion

The 27 groundwater samples and the 4 surface water samples were analysed using the HFE-D. The saltwater reference in HFE-D is considered, in this study, to be the Mediterranean Sea with its characteristic and documented concentrations in Ca^{2+}, Mg^{2+}, Na^+, K^+, HCO_3^-, SO_4^{2-}, and Cl^-. Figure 12a shows the distribution of hydrogeochemical facies in the HFE-D. The water samples affected by saltwater intrusion are underlined in red color, while samples presenting freshwater are underlined in green color. Fifteen (15) of the 27 groundwater samples were identified in the freshening stage, including 1 groundwater sample in the sub-stage f_3 corresponding to the Na-MixHCO_3 facies, and 14 groundwater samples were located in the freshening sub-stage f_4 indicating a facies of Ca-HCO_3. On the other hand, 12 groundwater samples were identified in the saltwater intrusion stage, including 9 groundwater samples in the sub-stage i_1 corresponding to the Ca-MixHCO_3 facies, 2 groundwater samples located in the saltwater sub-stage i_2 indicating a facies of Ca-MixCl, and 1 groundwater sample was identified in the saltwater sub-stage i_3 with a Na-Cl facies. The total number of groundwater samples impacted by saltwater represent a percentage of 44%. As can be seen in Figure 12a, the 4 surface water samples collected from the Guebli and Cherka Rivers (identified as 26, 27, 28, and 29) are mostly located in the saltwater sub-stage corresponding to the Na-Cl facies. This

location in the saltwater sub-stage can be explained by an interaction between these two rivers and the Mediterranean Sea, as they are directly connected. This finding is furthermore confirmed according to the WSDE graphical approach (WSDE, 2005), where the 4 surface water samples are plotted in the seawater intrusion area (Figure 12b). Furthermore, the groundwater samples, according to the WSDE graphical approach, could be divided into two main groups. The first group, ‘‘affected groundwater”, includes the groundwater samples affected by sea intrusion and the mixed groundwater, with a total of 11 groundwater samples; and a second group, characterized as ‘‘unaffected groundwater” contains 16 groundwater samples that fall in the normal water category. The number of groundwater samples affected by saltwater represent 41% of the entire data set considered in this study. For the SMI, the determined values of *T*, representing the inflection points from the cumulative probability curves for the concentrations of Na^+, Cl^-, Mg^{2+}, and SO_4^{2-} in groundwater samples (Figure 13), are 87 mg/L (Na^+), 98 mg/L (Cl^-), 18 mg/L (Mg^{2+}) and 93 mg/L (SO_4^{2-}). The surface water samples collected from the two rivers bordering the study area have not been considered during this part of the data processing, because the inflection points consider only the groundwater concentrations. Using these determined values of *T* in Eq. 2, the calculated SMI values range between 0.38 and 3.1, wherein 9 groundwater samples have shown a value of SMI exceeding 1, which indicates that groundwater is influenced by seawater mixing (Park et al., 2005). Therefore, 33% of the total groundwater samples can be considered to be affected by the mixing of seawater.

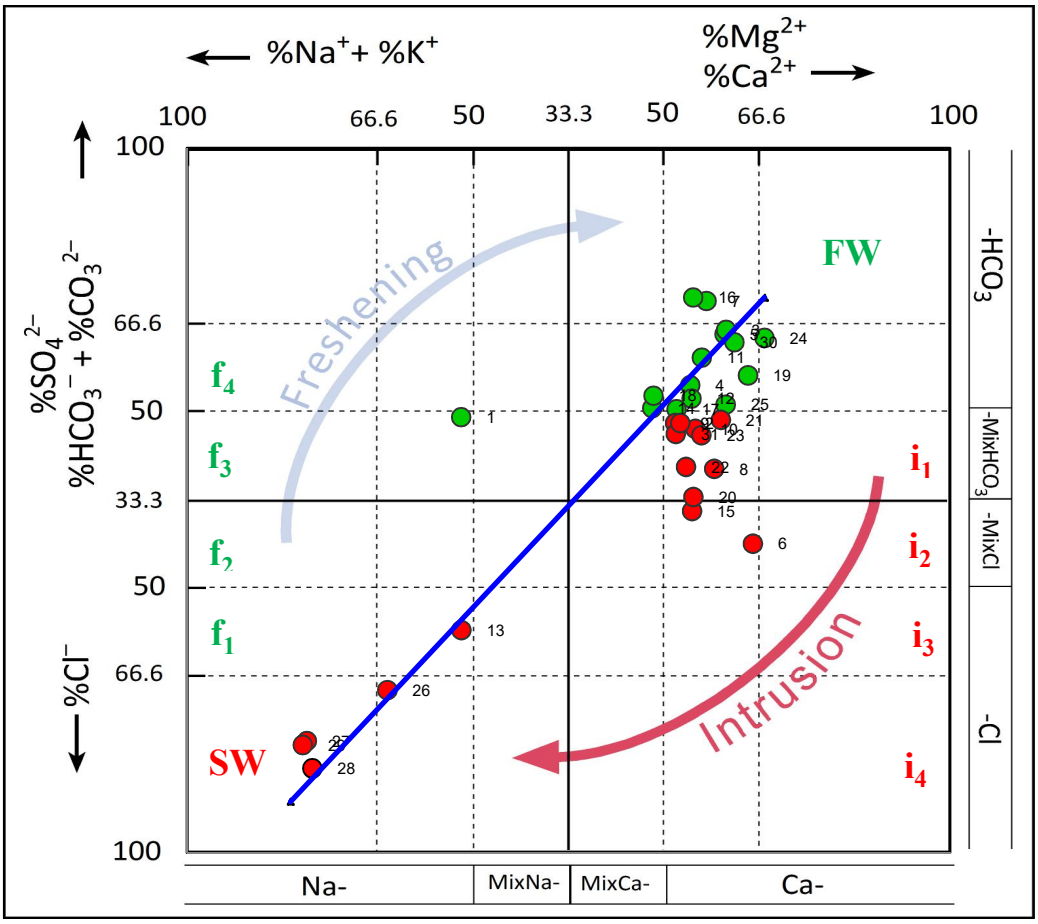
%Na+ + %K+
%Mg2+
%Ca2+
100
66.6
50
33.3
50
66.6
100
%SO4 2− + %HCO3− + %CO3 2−
%Cl−
FW
SW
Freshening
Intrusion
f4
f3
f2
f1
i1
i2
i3
i4
-HCO3
-MixHCO3
-MixCl
-Cl
Na-
MixNa-
MixCa-
Ca-

(a)

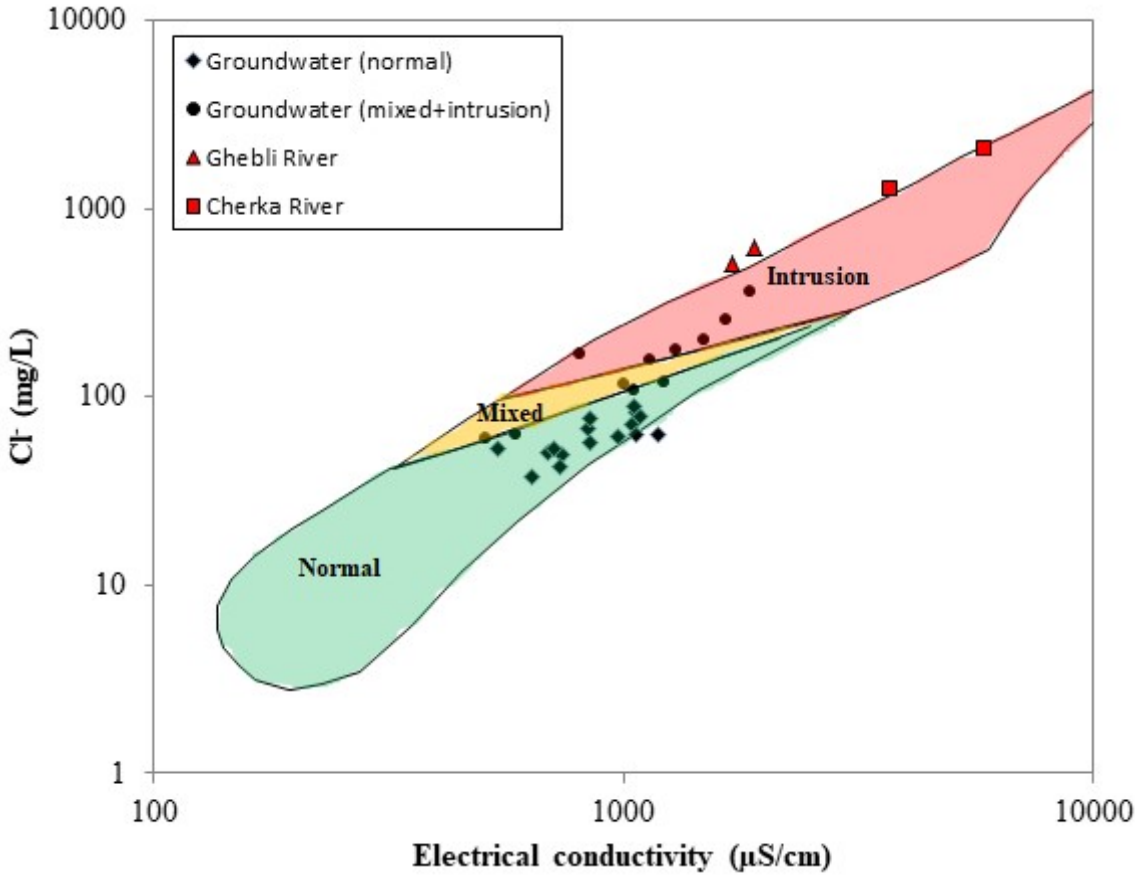

(b)

Figure 12. (a) Representation of all water samples by their number on the HFE-D, taking into account their position in relation to the intrusion and freshening sub-stages and CML; (b) Plotting of Cl-EC water samples on the WSDE's graphic approach.

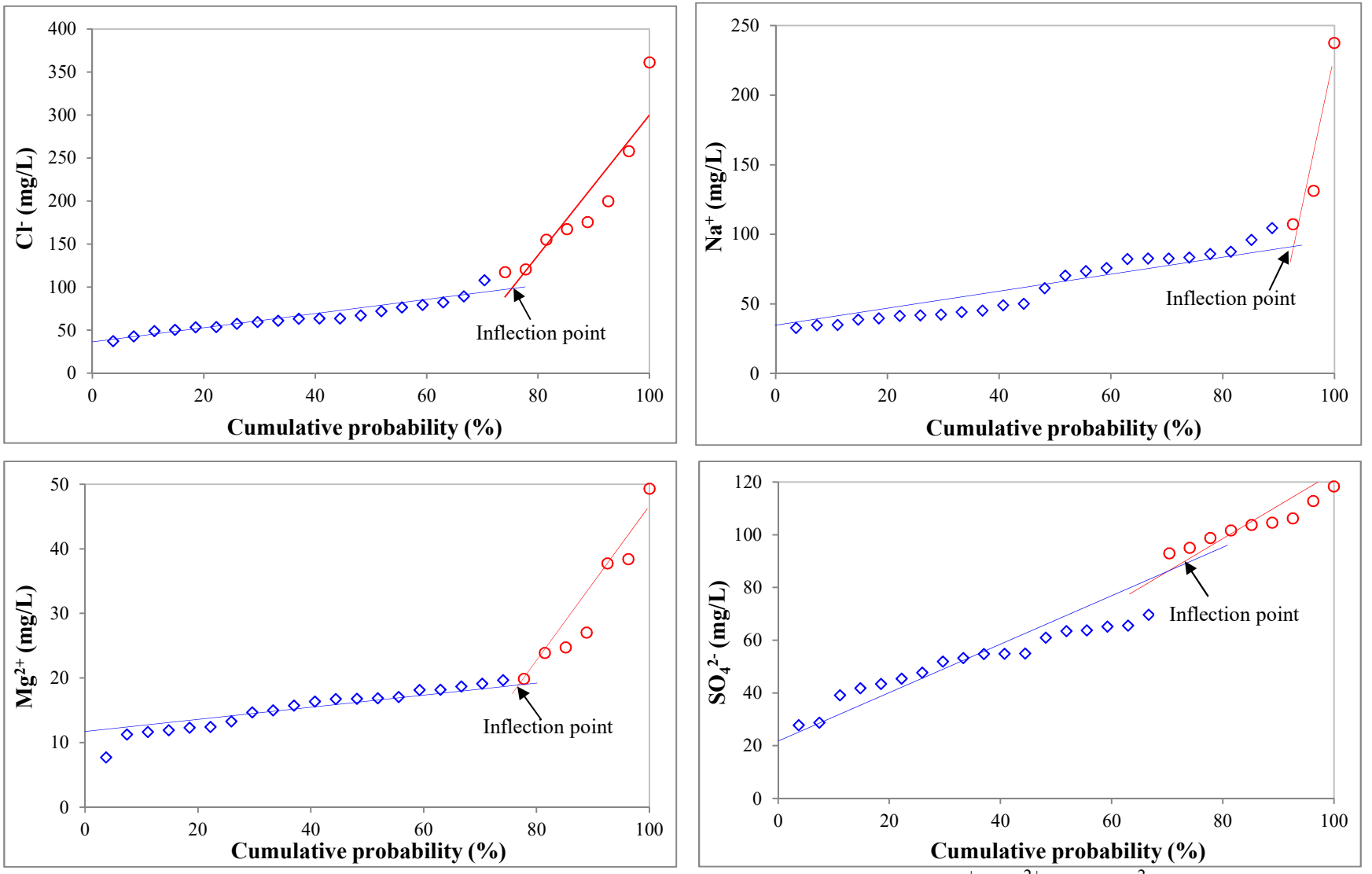

Figure 13. Interpretation of cumulative probability curves for the concentrations of Cl^-, Na^+, Mg^{2+}, and SO_4^{2-} in groundwater.

Table 5 presents the results of saltwater influence on groundwater chemistry according to the three methods used to determine saltwater influence. The number and corresponding percentage of the impacted groundwater samples vary between the three methods (HEF-D = 12 (44%), WSDE = 11 (41%), SMI = 9 (33%)). There is only a 3% difference (44% - 41%) between HEF-D and WSDE, compared to an 11% and an 8% difference recorded between HEF-D/SMI and WSDE/SMI, respectively. The 3 different methods do, however, show the same results for 10 unaffected groundwater samples, corresponding to 37% of the total number of groundwater samples (unaffected groundwater samples are: TAL-3, 5, 7, 11, 16, 17, 19, 24, 25, and 30 indicated in Table 5). As can be seen in the piezometric map presented in Figure 9, the location of these groundwater samples show overall high piezometric level. The locations of wells 7, 11, 16, 25 and 30, in particular, are marked by the highest groundwater level corresponding to the main fresh rainfall recharge locations as they are characterized by a classic Ca-HCO_3 groundwater type, indicative of recent recharge (Hiscock, 2009), that corresponds to freshening facies (Ghesquière et al., 2015). This finding is confirmed by a Gibbs's diagram (Gibbs, 1970), shown in Figure 14a, wherein the unaffected groundwater samples are grouped together as one set. Considering the locations of the unaffected wells in the study area (the location of all wells is shown in Figure 5), it could be assumed that they correspond to a transition zone between saltwater intrusion and water undergoing freshening, but mostly dominated by fresh rainfall water. The unaffected group in Gibbs's diagram (Figure 14a) also includes the groundwater samples TAL-21, 23 and 31 which were determined as being affected by saltwater according to HEF-D (Table 5). These three samples correspond to Ca-MixHCO_3 facies and are located close to the group of unaffected wells

(wells: 3, 5, 7, 11, 16, 17, 19, 24, 25 and 30) corresponding to facies Ca-HCO_3. The location of the three affected samples potentially corresponds to a transition zone between the unaffected groundwater characterized by Ca-HCO_3 and the affected groundwater characterized by a Ca-MixHCO_3 (Giménez-Forcada, 2010). The plotting of groundwater concentrations on the Piper's trilinear diagram (Piper, 1944) confirms the Ca-HCO_3 facies for unaffected groundwater (Figure 14b). By following the direction of groundwater flow from the zone corresponding to the unaffected wells to that of the affected wells, groundwater mainly changes from Ca-HCO_3 facies to mixed Ca-Cl facies. The change of water chemistry along the groundwater flow paths within the urban area suggests an anthropogenic influence, which can also be complemented by natural processes such as rainfall freshening (Erostate et al., 2018; Zendehbad et al., 2019).

Table 5. Comparison of the results obtained by the 3 different methods used in this study. "x" indicates that the groundwater sample has been identified as being affected by saltwater intrusion according to the method indicated at the top of the column.

	Methods		
Groundwater sample	HEF-D	WSDE	SMI
TAL-1		x	x
TAL-2	x	x	
TAL-3			
TAL-4		x	x
TAL-5			
TAL-6	x	x	x
TAL-7			
TAL-8	x		
TAL-9	x	x	
TAL-10	x	x	x
TAL-11			
TAL-12		x	x
TAL-13	x	x	x
TAL-14		x	x
TAL-15	x	x	x
TAL-16			
TAL-17			
TAL-18		x	x
TAL-19			
TAL-20	x		
TAL-21	x		
TAL-22	x		
TAL-23	x		
TAL-24			
TAL-25			
TAL-30			
TAL-31	x		

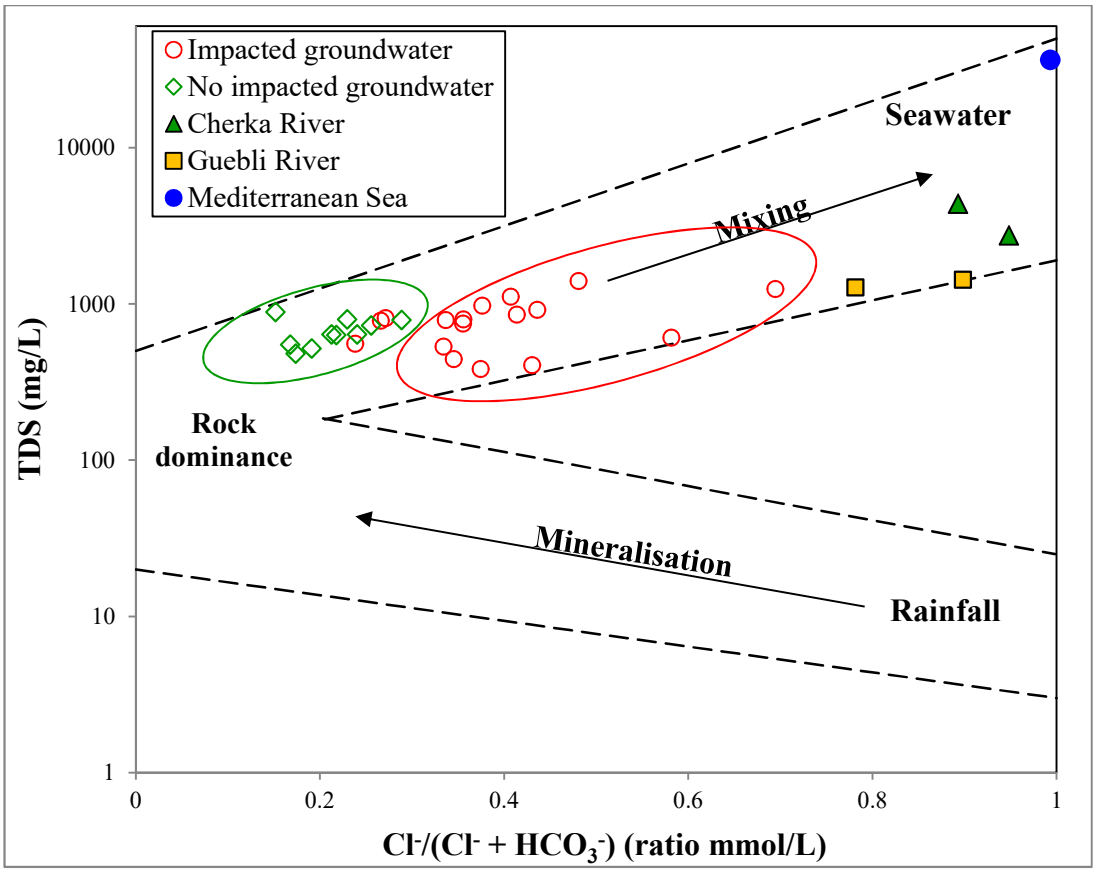
Impacted groundwater
No impacted groundwater
Cherka River
Guebli River
Mediterranean Sea
Seawater
Mixing
Rock dominance
Mineralisation
Rainfall
TDS (mg/L)
10000
1000
100
10
1
0
0.2
0.4
0.6
0.8
1
Cl-/(Cl- + HCO3-) (ratio mmol/L)

(a)

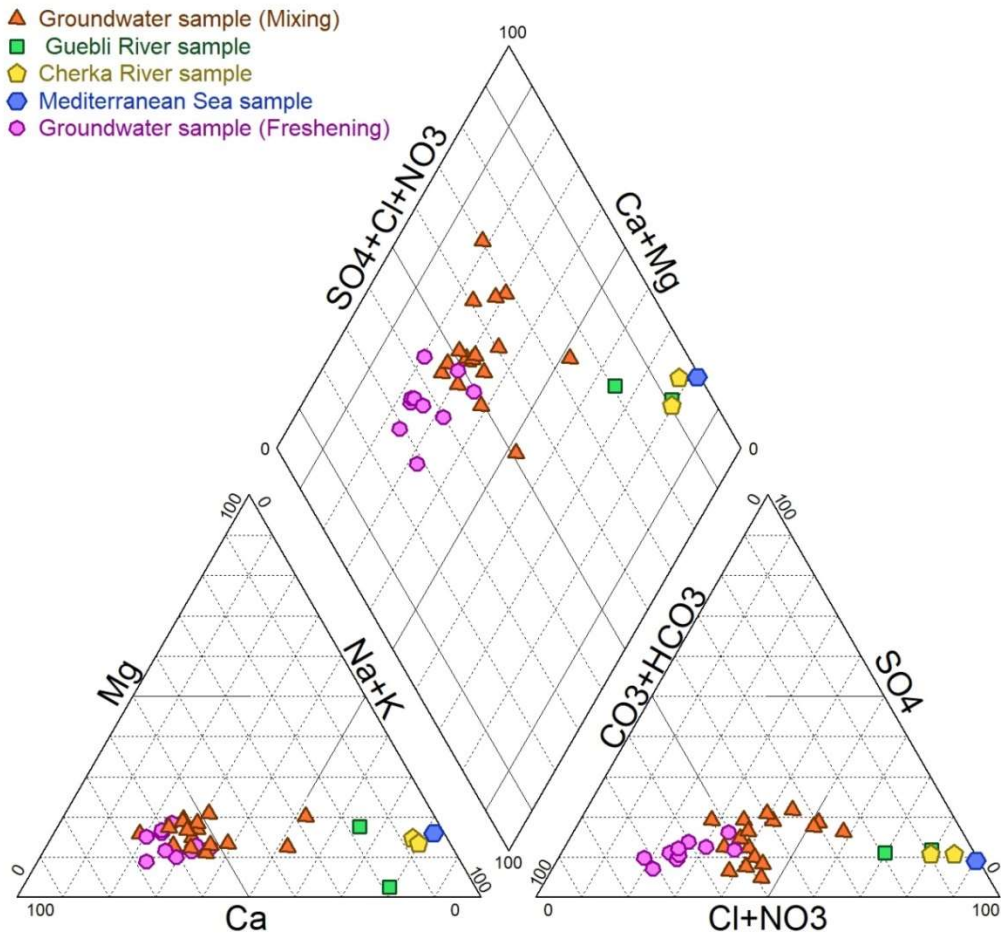

(b)

Figure 14. (a) Gibbs's diagram and (b) Piper's diagram for all water samples

4.4 **Effect of multi-source contamination on groundwater quality**

Based on the chemical and stable isotope analyses undertaken in the present study, the degradation of groundwater quality is due in large part to combined anthropogenic contamination originating from (i) saltwater intrusion induced by groundwater extraction, (ii) inadequate wastewater disposal systems and (iii) the use of manure-based fertilizers. These sources of contamination had already been observed in other elsewhere studies (e.g., Bouchaou et al., 2008; Christina et al., 2014; Mtoni et al., 2013; Najib et al., 2016;

Papazotos et al., 2017; Zghibi et al., 2013), but not in such combined way as observed in the present study. These results highlight the particularity of coastal aquifers as systems subjected to multi-sourced and cumulative stresses. The multi-origin contamination not only contributes to complex chemical reactions within the aquifer (Appelo and Postma, 2005), but it also contributes to affecting large sectors of the study area. Ten (10) of the 27 groundwater samples are observed to be unaffected by saltwater intrusion (TAL-3, 5, 7, 11, 16, 17, 19, 24, 25, and 30 - Table 5) according to the three evaluating methods used in the present study. Among these 10 groundwater samples (Figure 15), only three groundwater samples (TAL-3, 5, and 7) show moderate concentrations of nitrate (5 mg/L<NO_3^-<40 mg/L); and two groundwater samples (TAL-11 and 16) present nitrate concentrations ranging from 40 to 50 mg/L, while five groundwater samples (TAL-17, 19, 24, 25 and 30) present high concentrations of nitrate (NO_3^->50 mg/L). Hence, 50% of the groundwater samples that are unaffected by saltwater intrusion are instead mostly affected by nitrate concentrations exceeding the drinking water limit of 50 mg/L. Conversely, among the 11 groundwater samples (TAL-1, 3, 4, 5, 7, 9, 11, 12, 13, 16 and 18) presenting concentrations of nitrate below the drinking water limit of 50 mg/L (Figure 7), only five groundwater samples (TAL-3, 5, 7, 11 and 16) are determined to be unaffected by saltwater intrusion according to the three assessing methods used in the present study (Figure 15). Accordingly, approximately 60% of groundwater samples with nitrate concentrations lower than 50 mg/L are more affected by saltwater intrusion. The 10 groundwater samples deemed to be unaffected by saltwater intrusion according to the three evaluating methods used in the present study represent 37% of the 27 groundwater samples collected from the study area. Consequently, it can be considered that 63% of

groundwater samples are affected by saltwater intrusion. The 11 groundwater samples that reveal concentrations of nitrate below the drinking water limit of 50 mg/L represent 40% of the 27 groundwater samples collected from the study area. Consequently, it can be considered that 60% of groundwater samples are affected by concentrations of nitrate exceeding the drinking water limit of 50 mg/L. However, when the combined contamination is considered, a total of 22 of 27 groundwater samples are affected by some contamination; this representing 81% of groundwater samples collected from the study area.

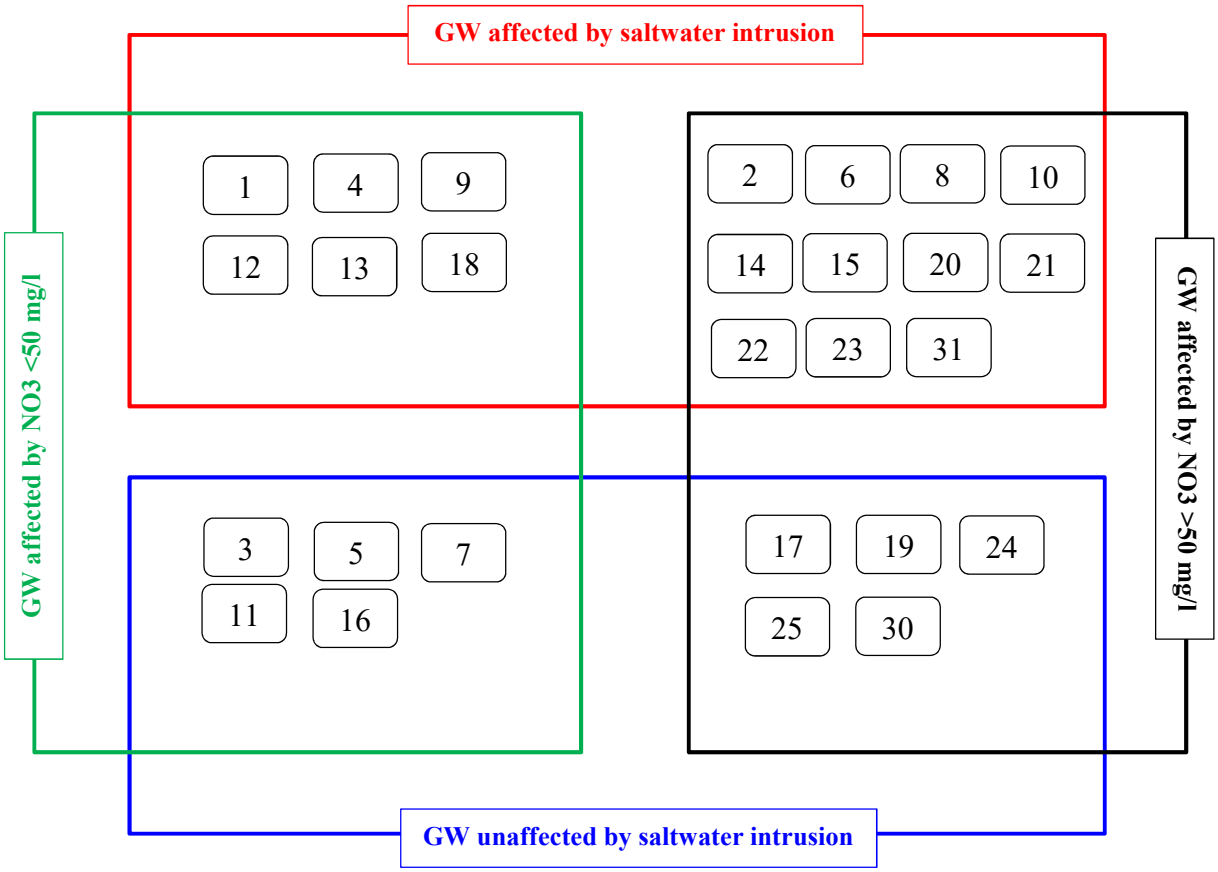

Figure 15. Illustration of the overlapping, crossed multi-source contamination on groundwater quality.

These findings show how the combined contamination contributes to affecting a large proportion of the aquifer. The spatial classified groundwater distribution presented in Figure 16 shows that the combined contamination is mostly revealed for the groundwater samples collected from wells located along the border of the study area. Here, it should be noted that at various times, the diffusion of the contamination within the study aquifer is supported by active groundwater flow. The piezometric map (Figure 9), representing the low-water period of June 2019, shows that groundwater flow is generally oriented from the center of the aquifer towards its borders. Such groundwater flow movement contributes particularly to more diffusion of nitrate-contaminated groundwater, as the nitrate-contaminated sectors are principally located in the central part of the study area. As an example, the affected groundwater samples TAL-24, 25, and 30, revealing high concentrations in nitrate (>50 mg/L), are located in the highly urbanized sector presenting inadequate private sanitation systems (see land-use map in Figure 3 and the locations of sampled wells in Figure 7). The groundwater samples TAL-31, 23, 15 also revealed high concentrations of nitrate (Figure 7), but they are located in a less urbanized sector compared to the immediate neighbouring highly urbanized sector where the wells TAL-24, 25, and 30 are located. Accordingly, it can be understood that groundwater, flowing from the highly urbanized sector towards the less urbanized sector (Figure 9), is directly contributing to nitrate diffusion which is confirmed by high nitrate concentrations in the less urbanized sector. Conversely, during the high-water period, inverse groundwater flow from the bordering rivers towards the aquifer (Boulabeiz 2006) contributes to saltwater diffusion via upstream migration of seawater through the river mouths.

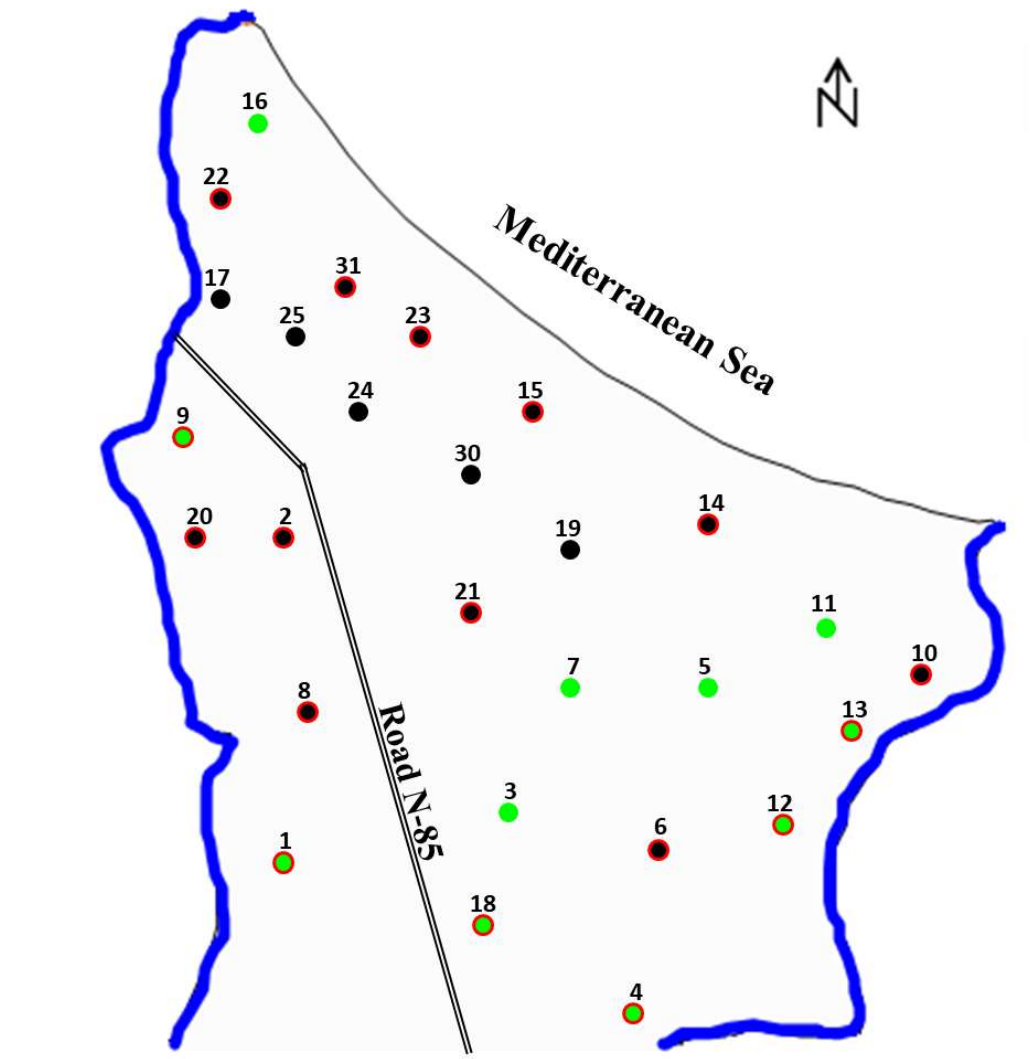

● Groundwater affected by NO_3^- <50 mg/l
● Groundwater affected by NO_3^- >50 mg/l
○ Groundwater affected by seawater intrusion

Figure 16. Spatial distribution of the classified groundwater.

5 Conclusion

The present study demonstrates that the combined analysis of chemical and isotopic indicators provides a solid basis for identifying the major processes controlling the degradation of groundwater in a coastal urban area subject to continuous population and

activity expansion and thus, to multiple sources of groundwater contamination. Results of this study of the coastal aquifer of Taleza (Algeria) highlight the close correlation that exists between urban sprawl and the marked increase of nitrate concentrations in groundwater. The study has also brought to light a particular issue affecting coastal areas, by delineating the key groundwater mineralization processes in effect. The continuous increase in nitrate concentrations observed in groundwater under sectors of high population density is directly linked to the continuous development of inadequate private sanitation systems over the expanding urban area. Low to moderate concentrations in nitrate were observed in groundwater under the cultivated sectors; these have been linked to animal manures, usually added to the soil before the start of the growing season to fertilize crops in agricultural areas. The impact of continuous and uncontrolled development practices, namely inefficient residential wastewater systems and the application of manure-based fertilizers, combined with low denitrification of groundwater in the study area, has led to a constant increase of nitrate over time. This has established a negative "nitrate legacy" in the aquifer, potentially threatening the future use of the groundwater resource at the regional scale. In addition, saltwater intrusion has been identified as a very active contributor to groundwater mineralization in the coastal aquifer of Taleza. The intrusion mechanism has been shown to be more complex than the simple and direct intrusion of the Mediterranean Sea into the aquifer, because (i) the study area is characterized by very specific interactions between saltwater and water originating from rainfall recharge that is undergoing freshening processes; and (ii) saltwater has been shown to be intruding through the river banks into the aquifer from the rivers bordering the study area during the high-water period and mixing with alluvial groundwater.

The effects of the anthropogenic groundwater contamination described in the present study have generated questions regarding the long-term protection of the aquifer on which the entire region is directly dependent for its water supply. Groundwater contamination started to become problematic over the last several decades, and is still strongly developing through an ever-increasing trend. The multiple sources of contamination identified in the present study (saltwater intrusion, inadequate wastewater systems and manure-based fertilizers), by their cumulative and combined effects, are affecting a large proportion of the study area. This phenomenon represents a continuous threat for the groundwater resource. Consequently, an optimization strategy of the groundwater extraction process, an introduction of environmentally safe agricultural practices and an implementation of regulations for managing wastewater in urbanized sectors are necessary to achieve a sustainable management of the groundwater potential of this Mediterranean coastal region.

Acknowledgements

The authors would like to thank Natural Sciences and Engineering Research Council of Canada (Discovery grant held by Prof. Romain Chesnaux) that have funded this project. The authors thank the local population of Taleza district, who provided much relevant information about the management of their wastewater, and offered free access to their private wells during fieldwork. Maxxam Laboratory in the Saguenay region of Quebec (Canada) is thanked for having provided sampling material including filters, luer-lock syringes and the amber glass bottles. The authors would like to thank Mr. Issam Boumaiza for his much-appreciated guidance and assistance during fieldwork. Dr.

Alexandra Mattei is thanked for her assistance in performing the water stable isotope analyses at the Hydrogeology Department of the University of Corsica in France. Ms. Josée Kaufmann is thanked for editorial collaboration.

6 References

Alcalá, F.J., Custodio, E., 2008. Using the Cl/Br ratio as a tracer to identify the origin of salinity in aquifers in Spain and Portugal. Journal of Hydrology 359, 189–207.

Alfarrah, N., Walraevens, K., 2018. Groundwater overexploitation and seawater intrusion in coastal areas of arid and semi-arid regions. Water (Switzerland) 10, 1–23.

ANRH, (Agence Nationale des Ressources Hydrauliques), 1974. Étude hydrogéologique de la plaine de Collo - Algérie. Département de l'Arrondissement de Constantine, Algérie.

Appelo, C.A.J., Postma, D., 2005. Geochemistry, groundwater and pollution, second edition, Geochemistry, Groundwater and Pollution. 2nd Edition, Balkema, Leiden, The Netherlands.

Aravena, R., Mayer, B., 2009. Isotopes and processes in the nitrogen and sulfur cycles, in: Environmental Isotopes in Biodegradation and Bioremediation. pp. 203–246.

Aravena, R., Robertson, W.D., 1998. Use of multiple isotope tracers to evaluate denitrification in ground water: Study of nitrate from a large-flux septic system plume. Ground Water 36, 975–982.

Argamasilla, M., Barberá, J.A., Andreo, B., 2017. Factors controlling groundwater salinization and hydrogeochemical processes in coastal aquifers from southern Spain. Science of the Total Environment 580, 50–68.

Baily, A., Rock, L., Watson, C.J., Fenton, O., 2011. Spatial and temporal variations in groundwater nitrate at an intensive dairy farm in South-East Ireland: Insights from stable isotope data. Agriculture, Ecosystems and Environment 144, 308–318.

Barthold, F.K., Tyralla, C., Schneider, K., Vaché, K.B., Frede, H.G., Breuer, L., 2011. How many tracers do we need for end member mixing analysis (EMMA)? A sensitivity analysis. Water Resources Research 47, 1–14.

Bear, J., Cheng, A.H.D., Ouazar, D., Sorek, S., Herrera, I., 1999. Seawater Intrusion in Coastal Aquifers-Concepts, Methods and Practices, Seawater Intrusion in Coastal Aquifers - Concepts, Methods and Practices. Kluwer Academic Publisher, Dordrecht, Boston, London.

Beeson, S., Cook, M.C., 2004. Nitrate in groundwater: A water company perspective. Quarterly Journal of Engineering Geology and Hydrogeology 37, 261–270.

Beloulou, L., 1987. hydrogeological study and evaluation of water resources of the Collo basin, Skikda, Algeria. Master's thesis, Arizona University, USA.

Bocanegra, E., da Silva, G.C., Custodio, E., Manzano, M., Montenegro, S., 2010. State of knowledge of coastal aquifer management in South America. Hydrogeology Journal 18, 261–267.

Böhlke, J.K., 2002. Groundwater recharge and agricultural contamination. Hydrogeology Journal 10, 153–179.

Böttcher, J., Strebel, O., Voerkelius, S., Schmidt, H.L., 1990. Using isotope fractionation of nitrate-nitrogen and nitrate-oxygen for evaluation of microbial denitrification in a sandy aquifer. Journal of Hydrology 114, 413–424.

Bouchaou, L., Michelot, J.L., Vengosh, A., Hsissou, Y., Qurtobi, M., Gaye, C.B., Bullen, T.D., Zuppi, G.M., 2008. Application of multiple isotopic and geochemical tracers for investigation of recharge, salinization, and residence time of water in the Souss-Massa aquifer, southwest of Morocco. Journal of Hydrology 352, 267–287.

Bouillin, J.P., 1979. La transversale de Collo et d'El Milia (Petite Kabylie) : une région-clef pour l'interprétation de la tectonique alpine de la chaine littorale d'Algérie. Memoires de la Societe Geologique de France, 57,3 (no. 135).

Bouillin, J.P., Kornprobst, J., 1974. Associations ultrabasiques de petite Kabylie: péridotite de type Alpin et complexe stratifié; comparaison avec les zones internes bético- rifaines. Bulletin de la société géologique de France, 7, 183–194.

Boulabeiz, M., 2006. Evolution des éléments chimiques et évaluation de risque des eaux souterraines à la pollution : Cas de la nappe de Collo, Nord-Est Algérien. Mémoire de Magister, Université d'Annaba, Algérie.

Boulabeiz, M., Stefan, K., Belgacem, H., Bousnoubra, H., 2018. GIS-based GALDIT method for vulnerability assessment to seawater intrusion of the Quaternary coastal Collo aquifer (NE-Algeria). Arabian Journal of Geosciences 11, 1–14.

Boumaiza, L., Chabour, N., Drias, T., 2019a. Is there still a chance to save the groundwater in Taleza aquifer ?, in: The Joint AGC/AMC/IAH-CNC Conference (May 12 to 15, 2019), Quebec City, (Quebec), Canada.

Boumaiza, L., Chabour, N., Drias, T., 2019b. Reviewing the potential anthropogenic sources of groundwater contamination - Case study of the expanding urban area of Taleza in Algeria, in: Proceedings of the 72nd Canadian Geotechnical Conference (GeoSt-John's 2019), Saint-John's, Newfoundland and Labrador, Canada,. p. 9.

Bouzourra, H., Bouhlila, R., Elango, L., Slama, F., Ouslati, N., 2015. Characterization of mechanisms and processes of groundwater salinization in irrigated coastal area using statistics, GIS, and hydrogeochemical investigations. Environmental Science and Pollution Research 22, 2643–2660.

Burden, R.J., 1982. Nitrate contamination of New Zealand aquifers: A review. N.Z. J. SCI. 25, 205–220.

Casciotti, K.L., Sigman, D.M., Hastings, M.G., Böhlke, J.K., Hilkert, A., 2002. Measurement of the oxygen isotopic composition of nitrate in seawater and freshwater using the denitrifier method. Analytical Chemistry 74, 4905–4912.

CGG, (Compagnie Générale de Géophysique), 1965. Étude géophysique dans la plaine de Collo - Algérie. Service du génie rural et de l'hydraulique agricole, Arrondissement de Constantine, Algérie.

Chabour, N., 2004. La surexploitation des eaux souterraines dans les plaines littorales : la nappe de Télezza dans la plaine de Collo (Nord-Est algérien). Sciences et Technologie 127–132.

Chabour, N., Benabbas, C., Bourefis, A., Kermandji, A., 2009. L'impact de l'étalement urbain sur les hydrosystèmes littoraux. Cas de la plaine de Collo (N-E Algérien). Annals of the University of Bucharest - Geography Series 39–48.

Chafouq, D., El Mandour, A., Elgettafi, M., Himi, M., Chouikri, I., Casas, A., 2018. Hydrochemical and isotopic characterization of groundwater in the Ghis-Nekor

plain (northern Morocco). Journal of African Earth Sciences 139, 1–13.
Chaouni, A.A., Halimi, N.E., Walraevens, K., Beeuwsaert, E., De Breuck, W., 1997. Investigation de la salinisation de la plaine de Bou-Areg (Maroc nord-oriental)., in: International Association of Hydrological Sciences, Freshwater Contamination. p. (243), 211-220.
Chatton, E., Aquilina, L., Pételet-Giraud, E., Cary, L., Bertrand, G., Labasque, T., Hirata, R., Martins, V., Montenegro, S., Vergnaud, V., Aurouet, A., Kloppmann, W., Pauwels, 2016. Glacial recharge, salinisation and anthropogenic contamination in the coastal aquifers of Recife (Brazil). Science of the Total Environment 569, 1114–1125.
Cheema, M.J.M., Immerzeel, W.W., Bastiaanssen, W.G.M., 2014. Spatial quantification of groundwater abstraction in the irrigated indus basin. Groundwater 52, 25–36.
Choudhury, K., Saha, D.K., Chakraborty, P., 2001. Geophysical study for saline water intrusion in a coastal alluvial terrain. Journal of Applied Geophysics 46, 189–200.
Christensen, T.H., Kjeldsen, P., Bjerg, P.L., Jensen, D.L., Christensen, J.B., Baun, A., Albrechtsen, H.J., Heron, G., 2001. Biogeochemistry of landfill leachate plumes. Applied Geochemistry 16, 659–718.
Christina, G., Konstantinos, S., Alexandros, G., Dimitrios, K., Aikaterini, K., 2014. Seawater intrusion and nitrate pollution in coastal aquifer of Almyros - Nea anchialos basin, central Greece. WSEAS Transactions on Environment and Development 10, 211–222.
Craig, H., 1961. Isotopic variations in meteoric waters. Science 133, 1702–1703.
Custodio, E., 2002. Aquifer overexploitation: What does it mean? Hydrogeology Journal 10, 254–277.
Davis, S.N., Fabryka-Martin, J.T., Wolfsberg, L.E., 2004. Variations of bromide in potable ground water in the United States. Ground Water 42, 902–909.
De-Camps, P., 1974. Estimation des ressources aquifères à l'aval de Oued Guebli, Skikda, Algeria. Direction des Études de Milieu et de la Recherche Hydraulique, Arrondissement de Constantine, Algérie.
Dindane, K., Bouchaou, L., Hsissou, Y., Krimissa, M., 2003. Hydrochemical and isotopic characteristics of groundwater in the Souss Upstream Basin, southwestern Morocco. Journal of African Earth Sciences 36, 315–327.
Drever, J.I., 1988. The Geochemistry of Natural Waters. Second ed. Prentice Hall, New Jersey.
Eissa, M.A., Thomas, J.M., Hershey, R.L., Dawoud, M.I., Pohll, G., Dahab, K.A., Gomaa, M.A., Shabana, A.R., 2014. Geochemical and isotopic evolution of groundwater in the Wadi Watir watershed, Sinai Peninsula, Egypt. Environmental Earth Sciences 71, 1855–1869.
Erisman, J.W., Sutton, M.A., Galloway, J., Klimont, Z., Winiwarter, W., 2008. How a century of ammonia synthesis changed the world. Nature Geoscience 1, 636–639.
Erostate, M., Huneau, F., Garel, E., Lehmann, M.F., Kuhn, T., Aquilina, L., Vergnaud-Ayraud, V., Labasque, T., Santoni, S., Robert, S., Provitolo, D., Pasqualini, V., 2018. Delayed nitrate dispersion within a coastal aquifer provides constraints on land-use evolution and nitrate contamination in the past. Science of the Total Environment 644, 928–940.
Fan, A.M., Steinberg, V.E., 1996. Health implications of nitrate and nitrite in drinking

water: An update on methemoglobinemia occurrence and reproductive and developmental toxicity. Regulatory Toxicology and Pharmacology 23, 35–43.
Faye, S., Maloszewski, P., Stichler, W., Trimborn, P., Faye, S.C., Gaye, C.B., 2005. Groundwater salinization in the Saloum (Senegal) delta aquifer: Minor elements and isotopic indicators. Science of the Total Environment 343, 243–259.
Ferah, S., 2015. Tourism durable et developpement local: Cas du village rural Taleza - Collo. Master's thesis, Université d'Annaba, Algérie.
Fukada, T., Hiscock, K.M., Dennis, P.F., 2004. A dual-isotope approach to the nitrogen hydrochemistry of an urban aquifer. Applied Geochemistry. https://doi.org/10.1016/j.apgeochem.2003.11.001
Garewal, S.K., Vasudeo, A.D., 2018. Causes and Sources of Groundwater Pollution: A Case Study of Nagpur City, India. In: Singh V., Yadav S., Yadava R. (eds) Groundwater. Water Science and Technology Library 76, 123–133.
Gat, J.R., Klein, B., Kushnir, Y., Roether, W., Wernli, H., Yam, R., Shemesh, A., 2003. Isotope composition of air moisture over the Mediterranean Sea: An index of the air-sea interaction pattern. Tellus, Series B: Chemical and Physical Meteorology 55, 953–965.
Ghesquière, O., Walter, J., Chesnaux, R., Rouleau, A., 2015. Scenarios of groundwater chemical evolution in a region of the Canadian Shield based on multivariate statistical analysis. Journal of Hydrology: Regional Studies 4, 246–266.
Gibbs, R.J., 1970. Mechanisms controlling world water chemistry. Science 170, 1088–1090.
Gilabert-Alarcón, C., Daesslé, L.W., Salgado-Méndez, S.O., Pérez-Flores, M.A., Knöller, K., Kretzschmar, T.G., Stumpp, C., 2018. Effects of reclaimed water discharge in the Maneadero coastal aquifer, Baja California, Mexico. Applied Geochemistry 92, 121–139.
Giménez-Forcada, E., 2019. Use of the Hydrochemical Facies Diagram (HFE-D) for the evaluation of salinization by seawater intrusion in the coastal Oropesa Plain: Comparative analysis with the coastal Vinaroz Plain, Spain. HydroResearch 2, 76–84.
Giménez-Forcada, E., 2010. Dynamic of sea water interface using hydrochemical facies evolution diagram. Ground Water 48, 212–216.
Giménez-Forcada, E., Sánchez San Román, F.J., 2015. An Excel Macro to Plot the HFE-Diagram to Identify Sea Water Intrusion Phases. Groundwater 53, 819–824.
Gooddy, D.C., Macdonald, D.M.J., Lapworth, D.J., Bennett, S.A., Griffiths, K.J., 2014. Nitrogen sources, transport and processing in peri-urban floodplains. Science of the Total Environment 494–495, 28–38.
Greer, F.R., Shannon, M., 2005. Infant methemoglobinemia: The role of dietary nitrate in food and water. Pediatrics 116, 784–786.
Grenet, B., 1972. Étude hydrogéologique de la plaine de Collo: Note synthétique sur les données acquises. DHW, Skikda, Algérie.
Gujer, W., Zehnder, J.B., 1983. Conversion Processes in Anaerobic Digestion. Water Science and Technology 15, 127–167.
Hamani, H., 1998. Étude hydrogéologique de la plaine de Collo par modèle mathématique. Mémoire de Magister, Université de Constantine, Algérie.
Han, D., Currell, M.J., 2018. Delineating multiple salinization processes in a coastal plain

aquifer, northern China: Hydrochemical and isotopic evidence. Hydrology and Earth System Sciences 22, 3473–3491.
Hiscock, K.M., 2009. Hydrogeology: principles and practice. Hoboken, NJ: John Wiley & Sons.
Huang, X., Deng, H., Zheng, C., Cao, G., 2016. Hydrogeochemical signatures and evolution of groundwater impacted by the Bayan Obo tailing pond in northwest China. Science of the Total Environment 543, 357–372.
Hudak, P.F., 2000. Regional trends in nitrate content of Texas groundwater. Journal of Hydrology 228, 37–47.
Jacob, C.E., 1947. Drawdown test to determine effective radius of artesian well. Transactions of the American Society of Civil Engineer 112, 1047–1070.
Jankowski, J., Acworth, R., Shekarforoush, S., 1998. Reverse ion-exchange in deeply weathered porphyritic dacite fractured aquifer system, Yass, New South Wales, Australia, in: 9th International Symposium on Water–Rock Interaction, Taupo, New Zealand. pp. 243–246.
Jin, Z., Pan, Z., Jin, M., Li, F., Wan, Y., Gu, B., 2012. Determination of nitrate contamination sources using isotopic and chemical indicators in an agricultural region in China. Agriculture, Ecosystems and Environment 155, 78–86.
Karroum, M., Elgettafi, M., Elmandour, A., Wilske, C., Himi, M., Casas, A., 2017. Geochemical processes controlling groundwater quality under semi arid environment: A case study in central Morocco. Science of the Total Environment 609, 1140–1151.
Kendall, C., 1998. Tracing Nitrogen Sources and Cycling in Catchments. Isotope Tracers in Catchment Hydrology 519–576.
Kendall, C., Elliott, E.M., Wankel, S.D., 2007. Tracing Anthropogenic Inputs of Nitrogen to Ecosystems, Chapter 12, In: R.H. Michener and K. Lajtha (Eds.). Stable Isotopes in Ecology and Environmental Science: Second Edition, Blackwell Publishing 375–449.
Ketabchi, H., Mahmoodzadeh, D., Ataie-Ashtiani, B., Simmons, C.T., 2016. Sea-level rise impacts on seawater intrusion in coastal aquifers: Review and integration. Journal of Hydrology 535, 235–255.
Khayat, S., Hötzl, H., Geyer, S., Ali, W., 2006. Hydrochemical investigation of water from the Pleistocene wells and springs, Jericho area, Palestine. Hydrogeology Journal 14, 192–202.
Kim, Y., Lee, K.S., Koh, D.C., Lee, D.H., Lee, S.G., Park, W.B., Koh, G.W., Woo, N.C., 2003. Hydrogeochemical and isotopic evidence of groundwater salinization in a coastal aquifer: A case study in Jeju volcanic island, Korea. Journal of Hydrology 270, 282–294.
Klassen, J., Allen, D.M., 2017. Assessing the risk of saltwater intrusion in coastal aquifers. Journal of Hydrology 551, 730–745.
Kopáček, J., Hejzlar, J., Posch, M., 2013. Factors controlling the export of nitrogen from agricultural land in a large central european catchment during 1900-2010. Environmental Science and Technology 47, 6400–6407.
Krom, F., 1965. Étude hydrogéologique de la plaine de Collo. DHW, Skikda, Algérie.
Langevin, C.D., Thorne Jr., D.T., Dausman, A.M., Sukop, M.C., Guo, W., 2007. SEAWAT Version 4: A Computer Program for Simulation of Multi-Species Solute

and Heat Transport, U.S. Geological Survey Techniques and Methods Book 6. Reston, USA: US Geological Survey.
Leaney, F.W., Herczeg, A.L., Walker, G.R., 2004. Groundwater Salinization in the South West Murray Basin as a Result of Enhanced Recharge, in: Origin of Salinity and Impacts on Fresh Groundwater Resources: Optimisation of Isotopic Techniques - Results of a 2000-2004 Coordinated Research Project. pp. 5–14.
Ledesma-Ruiz, R., Pastén-Zapata, E., Parra, R., Harter, T., Mahlknecht, J., 2015. Investigation of the geochemical evolution of groundwater under agricultural land: A case study in northeastern Mexico. Journal of Hydrology 521, 410–423.
Lemieux, J.M., Hassaoui, J., Molson, J., Therrien, R., Therrien, P., Chouteau, M., Ouellet, M., 2015. Simulating the impact of climate change on the groundwater resources of the Magdalen Islands, Québec, Canada. Journal of Hydrology: Regional Studies 3, 400–423.
Lu, Y., Tang, C., Chen, J., Sakura, Y., 2008. Impact of septic tank systems on local groundwater quality and water supply in the Pearl River Delta, China: case study. Hydrological Processes 22, 443–450.
Marre, A., 1987. Étude géomorphologique du Tell oriental algérien de Collo à la frontière tunisienne. Thèse doctorale, Université d'Aix-Marseille II, France.
Mas Pla, J., Ghiglieri, G., Uras, G., 2014. Seawater intrusion and coastal groundwater resources management: examples from two Mediterranean regions: Catalonia and Sardinia. Contributions to Science 10, 171–184.
Mason, C.F., 2002. Biology of freshwater pollution. 4th ed. Harlow, Essex: Prentice Hall.
Matiatos, I., 2016. Nitrate source identification in groundwater of multiple land-use areas by combining isotopes and multivariate statistical analysis: A case study of Asopos basin (Central Greece). Science of the Total Environment 541, 802–814.
Mayer, B., 2005. Assessing sources and transformations of sulphate and nitrate in the hydrosphere using isotope techniques, in: Isotopes in the Water Cycle: Past, Present and Future of a Developing Science. pp. 67–89.
MDDELCC, (Ministère du Développement durable de l'Environnement et de la Lutte contre les changements climatiques), 2015. Guide technique sur le traitement des eaux usées des résidences isolées. Règlement sur l'évacuation des eaux usées des résidences isolées. Québec, Canada.
Mecibah, I., 2008. Les ressources en eau et gestion intégrée du bassin versant d'Oued Guebli (Nord-Est Algérien). Mémoire de Magister, Université d'Annaba, Algérie.
Mengis, M., Schiff, S.L., Harris, M., English, M.C., Aravena, R., Elgood, R.J., MacLean, A., 1999. Multiple geochemical and isotopic approaches for assessing ground water NO3 - Elimination in a riparian zone. Ground Water 37, 448–457.
Meybeck, M., 1987. Global chemical weathering of surficial rocks estimated from river dissolved loads. American Journal of Science 287, 401–428.
Michael, H.A., Post, V.E.A., Wilson, A.M., Werner, A.D., 2017. Science, society, and the coastal groundwater squeeze. Water Resources Research 53, 2610–2617.
Minet, E.P., Goodhue, R., Meier-Augenstein, W., Kalin, R.M., Fenton, O., Richards, K.G., Coxon, C.E., 2017. Combining stable isotopes with contamination indicators: A method for improved investigation of nitrate sources and dynamics in aquifers with mixed nitrogen inputs. Water Research 124, 85–96.
Minmeliovodkhoz, K., 1968. Irrigation de la Plaine de Collo, Skikda (Algérie). Service

de la Direction d'Hydraulique de Skikda, Algérie.
Mtoni, Y., Mjemah, I.C., Bakundukize, C., Van Camp, M., Martens, K., Walraevens, K., 2013. Saltwater intrusion and nitrate pollution in the coastal aquifer of Dar es Salaam, Tanzania. Environmental Earth Sciences 70, 1091–1111.
Nair, I.S., Rajaveni, S.P., Schneider, M., Elango, L., 2015. Geochemical and isotopic signatures for the identification of seawater intrusion in an alluvial aquifer. Journal of Earth System Science 124, 1281–1291.
Najib, S., Fadili, A., Mehdi, K., Riss, J., Makan, A., Guessir, H., 2016. Salinization process and coastal groundwater quality in Chaouia, Morocco. Journal of African Earth Sciences 115, 17–31.
Nolan, B.T., 2001. Relating nitrogen sources and aquifer susceptibility to nitrate in shallow ground waters of the United States. Ground Water 39, 290–299.
Ntanganedzeni, B., Elumalai, V., Rajmohan, N., 2018. Coastal aquifer contamination and geochemical processes evaluation in Tugela Catchment, South Africa-Geochemical and statistical approaches. Water (Switzerland) 10, 1–22.
Panno, S.V., Hackley, K.C., Hwang, H.H., Kelly, W.R., 2001. Determination of the sources of nitrate contamination in karst springs using isotopic and chemical indicators. Chemical Geology 179, 113–128.
Panno, S.V., Kelly, W.R., Martinsek, A.T., Hackley, K.C., 2006. Estimating background and threshold nitrate concentrations using probability graphs. Ground Water 44, 697–709.
Papazotos, P., Koumantakis, I., Vasileiou, E., 2017. Seawater intrusion and nitrate pollution in coastal aquifer of Marathon basin. Bulletin of the Geological Society of Greece 50, 927–937.
Park, S.C., Yun, S.T., Chae, G.T., Yoo, I.S., Shin, K.S., Heo, C.H., Lee, S.K., 2005. Regional hydrochemical study on salinization of coastal aquifers, western coastal area of South Korea. Journal of Hydrology 313, 182–194.
Parkhurst, D.L., Appelo, C.A.J., 1999. User's Guide to PHREEQC (Version 2): A Computer Program for Speciation, Batch-Reaction, One-Dimensional Transport, and Inverse Geochemical Calculations, Water-Resources Investigations Report 99-4259.
Pastén-Zapata, E., Ledesma-Ruiz, R., Harter, T., Ramírez, A.I., Mahlknecht, J., 2014. Assessment of sources and fate of nitrate in shallow groundwater of an agricultural area by using a multi-tracer approach. Science of the Total Environment 855–864.
Piper, A.M., 1944. A graphic procedure in the geochemical interpretation of water-analyses. Eos, Transactions American Geophysical Union 25, 914–928.
Pool, M., Carrera, J., 2011. A correction factor to account for mixing in Ghyben-Herzberg and critical pumping rate approximations of seawater intrusion in coastal aquifers. Water Resources Research 47, 1–9.
Post, V.E.A., 2005. Fresh and saline groundwater interaction in coastal aquifers: Is our technology ready for the problems ahead? Hydrogeology Journal 13, 120–123.
Rajmohan, N., Elango, L., 2004. Identification and evolution of hydrogeochemical processes in the groundwater environment in an area of the Palar and Cheyyar River Basins, Southern India. Environmental Geology 46, 47–61.
Rao, N.S., 2006. Nitrate pollution and its distribution in the groundwater of Srikakulam district, Andhra Pradesh, India. Environmental Geology 51, 631–645.
Rivett, M.O., Buss, S.R., Morgan, P., Smith, J.W.N., Bemment, C.D., 2008. Nitrate

attenuation in groundwater: A review of biogeochemical controlling processes. Water Research 42, 4215–4232.
Ros, S.E.M., Zuurbier, K.G., 2017. The impact of integrated aquifer storage and recovery and brackish water reverse osmosis (ASRRO) on a coastal groundwater system. Water (Switzerland) 9, 1–20.
Rust, C.M., Aelion, C.M., Flora, J.R.V., 2000. Control of pH during denitrification in subsurface sediment microcosms using encapsulated phosphate buffer. Water Research 34, 1447–1454.
Rusydi, A.F., 2018. Correlation between conductivity and total dissolved solid in various type of water: A review, in: IOP Conference Series: Earth and Environmental Science. pp. 118–012019.
Sdao, F., Parisi, S., Kalisperi, D., Pascale, S., Soupios, P., Lydakis-Simantiris, N., Kouli, M., 2012. Geochemistry and quality of the groundwater from the karstic and coastal aquifer of Geropotamos River Basin at north-central Crete, Greece. Environmental Earth Sciences 67, 1145–1153.
Seddique, A.A., Masuda, H., Anma, R., Bhattacharya, P., Yokoo, Y., Shimizu, Y., 2019. Hydrogeochemical and isotopic signatures for the identification of seawater intrusion in the paleobeach aquifer of Cox's Bazar city and its surrounding area, south-east Bangladesh. Groundwater for Sustainable Development 9, 1–12.
Seiler, R.L., 2005. Combined use of 15N and 18O of nitrate and 11B to evaluate nitrate contamination in groundwater. Applied Geochemistry 20, 1626–2163.
Senthilkumar, S., Gowtham, B., Sundararajan, M., Chidambaram, S., Lawrence, J.F., Prasanna, M.V., 2018. Impact of landuse on the groundwater quality along coastal aquifer of Thiruvallur district, South India. Sustainable Water Resources Management 4, 849–873.
Shi, X., Wang, Y., Jiao, J.J. imm., Zhong, J., Wen, H., Dong, R., 2018. Assessing major factors affecting shallow groundwater geochemical evolution in a highly urbanized coastal area of Shenzhen City, China. Journal of Geochemical Exploration 184, 17–27.
Shuler, C.K., El-Kadi, A.I., Dulai, H., Glenn, C.R., Fackrell, J., 2017. Source partitioning of anthropogenic groundwater nitrogen in a mixed-use landscape, Tutuila, American Samoa. Hydrogeology Journal 25, 2419–2434.
Sigman, D.M., Casciotti, K.L., Andreani, M., Barford, C., Galanter, M., Böhlke, J.K., 2001. A bacterial method for the nitrogen isotopic analysis of nitrate in seawater and freshwater. Analytical Chemistry 73, 4145–4153.
Sinclair, A.J., 1974. Selection of threshold values in geochemical data using probability graphs. Journal of Geochemical Exploration 3, 129–149.
Singh, B., Singh, Y., Sekhon, G.S., 1995. Fertilizer-N use efficiency and nitrate pollution of groundwater in developing countries. Journal of Contaminant Hydrology 20, 167–184.
Singleton, M.J., Esser, B.K., Moran, J.E., Hudson, G.B., Mcnab, W.W., Harter, T., 2007. Saturated zone denitrification: Potential for natural attenuation of nitrate contamination in shallow groundwater under dairy operations. Environmental Science and Technology 41, 759–765.
Steyl, G., Dennis, I., 2010. Review of coastal-area aquifers in Africa. Hydrogeology Journal 18, 217–225.

Stigter, T.Y., Van Ooijen, S.P.J., Post, V.E.A., Appelo, C.A.J., Carvalho Dill, A.M.M., 1998. A hydrogeological and hydrochemical explanation of the groundwater composition under irrigated land in a Mediterranean environment, Algarve, Portugal. Journal of Hydrology 208, 262–279.

Stoewer, M.M., Knöller, K., Stumpp, C., 2015. Tracing freshwater nitrate sources in pre-alpine groundwater catchments using environmental tracers. Journal of Hydrology 524, 753–767.

Sutton, M.A., Howard, C.M., Erisman, J.W., Billen, G., Bleeker, A., Grennfelt, P., Van Grinsven, H., Grizzetti, B., 2011. The European Nitrogen Assessment, The European Nitrogen Assessment. Cambridge University Press.

Vitousek, P.M., Aber, J.D., Howarth, R.W., Likens, G.E., Matson, P.A., Schindler, D.W., Schlesinger, W.H., Tilman, D.G., 1997. Human alteration of the global nitrogen cycle: Sources and consequences. Ecological Applications 7, 737–750.

Vystavna, Y., Diadin, D., Yakovlev, V., Hejzlar, J., Vadillo, I., Huneau, F., Lehmann, M.F., 2017. Nitrate contamination in a shallow urban aquifer in East Ukraine: evidence from hydrochemical, stable isotopes of nitrate and land use analysis. Environmental Earth Sciences 76, 1–13.

Wakida, F.T., Lerner, D.N., 2005. Non-agricultural sources of groundwater nitrate: A review and case study. Water Research 39, 3–16.

Walter, J., Chesnaux, R., Cloutier, V., Gaboury, D., 2017. The influence of water/rock − water/clay interactions and mixing in the salinization processes of groundwater. Journal of Hydrology: Regional Studies 13, 168–188.

Wang, S., Zheng, W., Currell, M., Yang, Y., Zhao, H., Lv, M., 2017. Relationship between land-use and sources and fate of nitrate in groundwater in a typical recharge area of the North China Plain. Science of the Total Environment 609, 607–620.

Wassenaar, L.I., 1995. Evaluation of the origin and fate of nitrate in the Abbotsford Aquifer using the isotopes of15N and18O in NO3-. Applied Geochemistry 10, 391–405.

Werner, A.D., 2010. A review of seawater intrusion and its management in Australia. Hydrogeology Journal 18, 281–285.

Werner, A.D., Bakker, M., Post, V.E.A., Vandenbohede, A., Lu, C., Ataie-Ashtiani, B., Simmons, C.T., Barry, D.A., 2013. Seawater intrusion processes, investigation and management: Recent advances and future challenges. Advances in Water Resources 51, 3–26.

WHO, (World Health Organization), 2017. Guidelines for drinking-water quality, 4th edition, incorporating the 1st addendum. ISBN: 978-92-4-154995-0.

WSDE, (Washington State Department of, 2005. Water Resource Inventory Area 06 Islands. Seawater Intrusion. Topic Paper (https://fortress.wa.gov/ecy/publications/SummaryPages/1203271.html).

Zendehbad, M., Cepuder, P., Loiskandl, W., Stumpp, C., 2019. Source identification of nitrate contamination in the urban aquifer of Mashhad, Iran. Journal of Hydrology: Regional Studies 25.

Zghibi, A., Tarhouni, J., Zouhri, L., 2013. Assessment of seawater intrusion and nitrate contamination on the groundwater quality in the Korba coastal plain of Cap-Bon (North-east of Tunisia). Journal of African Earth Sciences 87, 1–12.